
System design of a geothermal sourced CO₂ network in a residential district

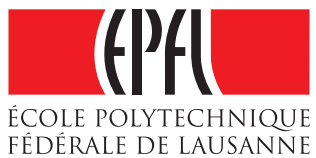
Master thesis at IPESE, Sion

Tobia Wyss^{*2}, Amorim Leandro De Castro Amoedo Rafael ^{†1}, Luc Girardin^{‡1}, and François Maréchal^{§1}

¹*Industrial Process and Energy Systems Engineering (IPESE), EPFL*

²*Master Student, Energy Management and Sustainability , EPFL*

April 9, 2019



^{*}tobia.wyss@epfl.ch

[†]rafael.amoedo@epfl.ch

[‡]luc.girardin@epfl.ch

[§]francois.marechal@epfl.ch

Abstract

Many countries and cities in the world have pledged to drastically reduce their CO₂ emissions during the next decades. Given the high degree of urbanization in occidental society, district energy systems present a high potential to increase the efficiency of heating and cooling systems. The present work focuses on a specific type of district network, based on CO₂ as a working fluid, which allows to exchange heat through condensation and evaporation. The low distribution temperature increases the potential of heat recovery, and thus the energy and exergy efficiency of the global system. Previous studies have shown that very high efficiencies can be reached with the use of heat pumps to supply heat to the buildings, and harvesting heat from lake water. The aim of this work is to study the performance of such a system, based on a case study, the Eglantine district located near Lausanne. The focus is set at evaluating the integration of a geothermal field, as a heat source. The main research questions that will be tried to answer are:

How does the CO₂ district energy network perform - energetically as well as financially - in the Eglantine district, and under which conditions does it perform better than concurrent solutions?

What are the characteristics of a typical district that favor the choice of the CO₂ district energy network technology?

The results show a very high energy and exergy performance (COP_{global} of 6.1) for the CO₂ network that is combined with a geothermal field, which is considerably higher than for the conventional GS-HP system (COP_{global} of 4.6). The difference is principally explained by the use of a direct expansion system of CO₂ into the ground. Moreover, it is shown that for different uses of the buildings there is an optimal ground temperature, or in other words an optimal borehole depth, and the other way around. This work identifies the key parameters that the CO₂ network technology can leverage to compete against modern, well performing, heat pump systems.

Acknowledgments

I would like to thank prof. Marechal to have given me the opportunity to do my master thesis in his research group IPESE, on a subject and in a mindset that i appreciate a lot.

I had the chance to work with Rafael Amoedo and Luise Middelhauve, who i thank for having supervised me and, most importantly, for having given me a good support and structure. A special thanks goes to Luc Girardin for the useful and interesting discussions we had, but also for the time he accorded me and the guidance given me throughout this project.

I also thank all the other doctor students and researchers at IPESE that might have answered some of my questions, or simply greeted me in the morning. It was a pleasure!

Contents

1	Introduction	1
1.1	Context	1
1.2	Scope	2
2	State of the art	3
2.1	District heating	3
2.2	Fifth generation district energy networks	3
2.3	CO ₂ district energy network	5
2.3.1	The technology	5
2.3.2	Performance	7
2.3.3	Integration in smart energy system	7
2.4	Direct-expansion ground source heat pump	8
3	Methodology	11
3.1	Energy demand - Typical days	11
3.2	Geothermal wells	11
3.3	Investment cost function	11
3.4	Minimum approach temperature	12
3.5	Exergy	13
3.6	Energy technology models	14
3.6.1	Heat pump - Carnot cycle	14
3.6.2	Heat pump - Thermodynamic cycle	14
3.6.3	Heat pump - Supercritical CO ₂	16
3.6.4	Outdoor condensing unit	18
3.6.5	Geo-cooling	18
3.6.6	PV	18
3.6.7	Network	18
3.7	MILP optimization and Osmose	19
4	Application	21
4.1	Case-study Eglantine	21
4.1.1	Context	21
4.1.2	Available data	22
4.1.3	Energy demand - Typical days	23
4.2	Heat sources	23
4.2.1	Stream	23
4.2.2	Lake	24
4.2.3	Geothermal wells	24
4.3	External heat sources	25
4.3.1	Ice rink	25
4.4	PV	27
4.5	Energy conversion technologies	28
4.5.1	GS-HP	28
4.5.2	CO ₂ DEN	29
4.6	Numerical application	31
4.6.1	Cost functions	31
4.6.2	Minimum approach temperature	32
4.6.3	Compressor efficiencies	32
4.6.4	Direct expansion HP	33
4.6.5	Recalculation of the COP efficiency	33

5 Results and discussion	35
5.1 Energy and exergy performance	35
5.2 Financial analysis	36
5.2.1 Parametric optimization of GS-HP	38
5.2.2 Parametric optimization of GS-CO2DEN	39
5.3 Heat source integration	40
5.4 Ground temperature response	42
5.5 Lake distance	43
5.6 Optimization of energy demand	43
6 Conclusions and outlook	52
A Anergy nets Switzerland	57
B Call for tender Eglantine - details	60
C CO2DEN	62
D Geothermal analysis for the Lemanic region	63
E Geothermal models	65

Glossary

Acronyms

AC	Air cooling
CAPEX	Capital Expenditure
CFC	Chlorofluorocarbons
CHP	Combined Heat and Power
COP	Coefficient of performance
CP	Central Plant
DEN	District Energy Network
DH	District Heating
DHC	District Heating and cooling
DHW	Domestic Hot Water
DSM	Demand Side Management
DX	Direct Expansion
EER	Energy Efficiency Ratio
ERA	Energy Reference Area
EX	Heat exchanger
GC	Geo-cooling
GS-HP	Ground sourced HP
HCFC	Hydrochlorofluorocarbon
HE	Heat Exchanger
HFC	Hydrofluorocarbons
HFO	Hydrofluoroolefin
HP	Heat Pump
IC	Investment Cost
LMTD	Logarithmic mean temperature difference
LS-HP	Lake sourced HP
MILP	Mixed Integer Linear Programming
OC	Operating Cost
OPEX	Operational Expenditure
PtG	Power To Gas
PV	Photovoltaics
R-EL	Electric heater
REF	Refrigeration
SH	Space Heating
TC	Total Cost

Indices

<i>amb</i>	ambient
<i>comp</i>	compressor
<i>cond</i>	condensation
<i>evap</i>	evaporation
<i>is</i>	isentropic
<i>liq</i>	liquid
<i>mech</i>	mechanical
<i>ref</i>	refrigerant
<i>sc</i>	subcooling
<i>sh</i>	superheating
<i>summer</i>	Summer conditions (cooling season)
<i>vap</i>	vapor
<i>winter</i>	Winter conditions (heating season)

Superscripts

+	Positive entering the system
-	Positive leaving the system

1 Introduction

1.1 Context

Throughout the last decades, human society has developed thanks to energy, most of which has come from fossil fuels. This has led to an unprecedented rise in CO₂ emissions, which have proved to be at the source of climate change. In order to secure a livable planet for the years to come, it is necessary, among others, to drastically reduce CO₂ emissions [1]. Since the adoption of the Kyoto protocol, the first international treaty about the fight against climate change in 1992, many countries have agreed to drastically reduce CO₂ emissions in the coming decades.

One crucial sector is the production of heat, which represents a large share of the total greenhouse emissions [2]. This is especially true for countries at higher latitudes, i.e. with cold climates. For example in Switzerland the energy demand for space heating and hot water demand of buildings, accounts for around 41% (96.5 TWh) of the total energy demand of the country, and is still strongly dependent from fossil fuels. This value rises to 54% (123.9 TWh) if process heat is included.

The energy demand related to cooling is experiencing an exponential growth. This is, on the one hand, because it is becoming affordable for more people, as income levels rise. On the other hand, this increase is due to global warming, which leads worldwide to a higher average temperature, as well as an increase in the frequency of days with extreme temperatures [1]. In some countries, especially in the Middle East, as well as in parts of the USA, during extremely hot days cooling can represent more than 70% of peak residential electricity demand. A huge problem with respect to this, is the quality of ACs. The majority of ACs that are sold in large markets have an efficiency that is only 50% or lower than the one of the best products available. This engenders, obviously, an important augmentation of the energy demand. Figure 1 shows how the energy demand has tripled since 1990, while the share of cooling energy in total energy use in buildings has risen from 2% to more almost 7% [3].

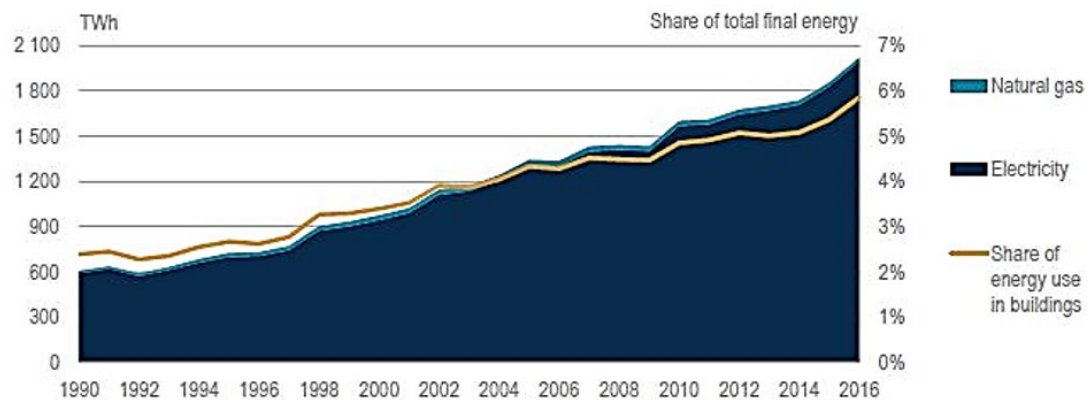


Figure 1: World energy consumption for space cooling in buildings. Source:[3]

A study shows that also in Switzerland cooling demand will strongly increase in the next decades, due to climate change. Figure 2 shows how this is particularly true for modern houses, which are very well insulated and efficient for the winter use. In this case the cooling demand will represent more or less a third of the heating demand [4].

According to the Population Division of the United Nations, the share of the world population living in cities has steadily increased from 34% in 1960 to 55% in 2017. Moreover, they prospect that, by 2050, this number will rise to 66%. In Switzerland, as well as in its neighbouring countries, the percentage of urban population is considerably higher, with 74% (2017) [5]. The fact that people live more and more in concentrated areas, also means that the density of energy consumption is rising. This becomes particularly interesting for urban heating and cooling demand, since the high density of heat consumers sets the conditions for efficient systems, based on district energy

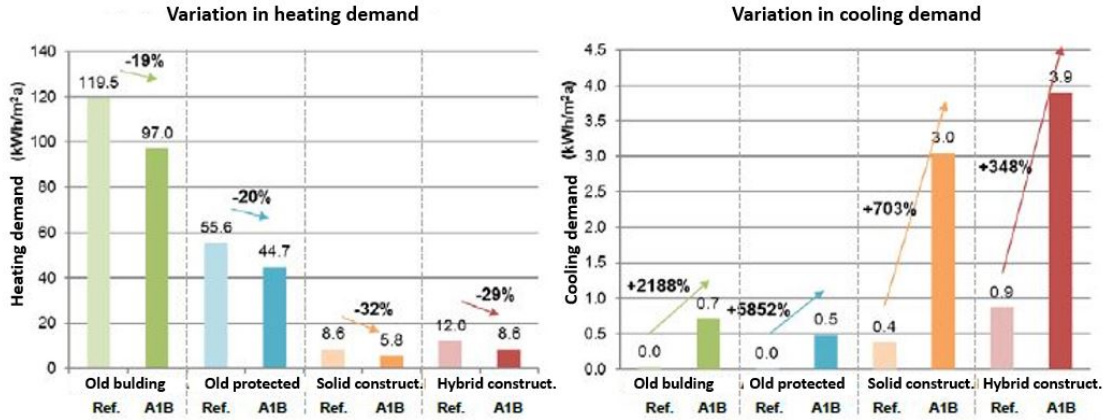


Figure 2: The evolution of median values of heating (left) and cooling (right) demand of the fours case studies ("Old building", "Old builing protected", "Solid construction", "Hybrid construction") between the reference period "1995" (1980-2009) and the period "2060" (2045-2074) in Basel. The percentage variations can be attributed to climate change. A1B corresponds to a median scenario developed by the IPCC. Source: [4]

networks.

The UNEP (United Nations Environment Programme) has identified a big potential in modern district energy systems, as the most effective approach to improve energy efficiency for heating and cooling, and enable the integration of renewable energies. However, these technologies require a high level of technology coordination and planning, since they create more efficient systems that are also more complex to deploy and operate. This is why, further research and technology development are needed in order to foster the spreading of these technologies.

1.2 Scope

The scope of this project is to pursue the study of the application of the CO₂ based district energy network technology, proposed by Weber and Favrat [6]. In collaboration with Romande Energie, the utility company of canton Vaud, a feasibility study was performed on a specific case study: the residential district Eglantine in Morges. The work tried to answer the main research questions:

How does the CO₂ district energy network perform - ecologically as well as financially - in the Eglantine district, and under which conditions does it perform better than concurrent solutions?

What are the characteristics of a typical district that favor the choice of the CO₂ district energy network technology?

2 State of the art

2.1 District heating

The evolution of district heating (DH) is shown in Figure 3. The first District Heatings (DH) have been installed in the 1880s in the USA, using concrete ducts to distribute steam at high temperature, which was then condensated by the consumers. This system was obviously not very efficient, due to the elevated heat losses during transportation, as well as the exergy losses due to the high temperature level. In the early 1930 a second generation was developed, which was based on the use of pressurized water, distributed above 100°C. These networks were installed with the purpose of reducing fuel consumption, as well as to integrate the energy generation through CHPs (Combined Heat and Power). The third generation was introduced in the 1980s and it's main difference was the use of a lower distribution temperature (below 100 °C). In those years the main reasons for the installation of DH was security of supply, since they allowed to replace oil with more local and cheaper fuels such as coal, biomass and waste. Moreover, it allowed to use industrial waste heat, as an energy source.

Nevertheless, a distribution temperature between 70-100 °C still origins very high heat losses, and it does not allow to integrate a larger number of heat sources. Moreover, also in space heating systems in buildings, there has been an evolution towards lower operating temperatures, reducing the average demand temperature. These were the drivers for the development of the 4th generation, for which networks operate at a temperature between 30-70 °C. This enables a much better integration of the heating system into the global energy system, as it makes it possible to include low temperature sources (geothermal, solar thermal, refrigeration systems or waste heat from data centers).

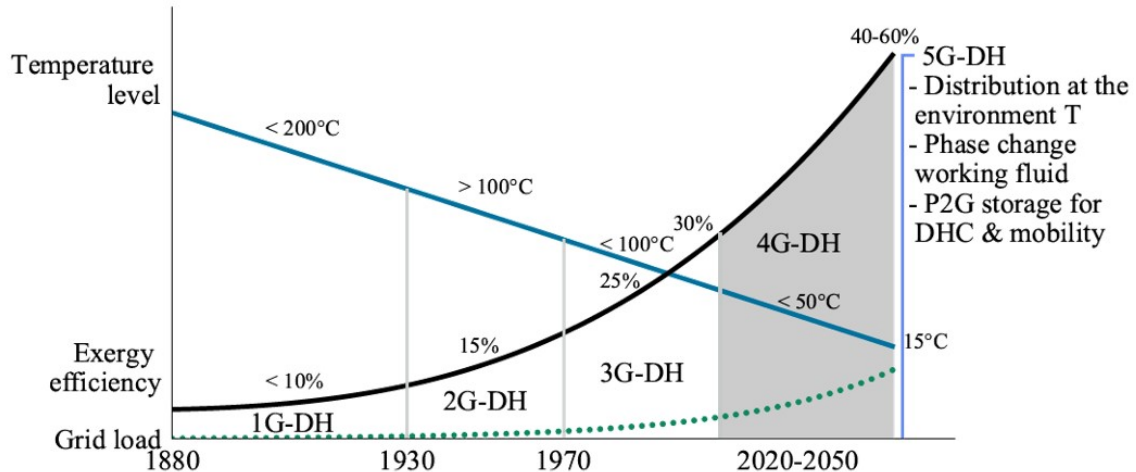


Figure 3: The evolution of the district heating technology. Source:[7]

2.2 Fifth generation district energy networks

The 4th generation of DH technology, has already achieved remarkable success and has been widely applied, especially in Europe. However, the exergy losses of the system are still very high, due to the diversity of heat levels present in the system, limiting its efficiency. Moreover, the integration of DC, which will become more and more important throughout the next decades, needs the installation of a second and separate networks, which leads to high upfront costs.

This has lead to the birth of a new technology that uses an even lower distribution temperature (10-25 °C) to provide heating and cooling. In fact, the transfer fluid acts as cold network for cooling purposes and supplies, at the same time, evaporator heat to decentralized heat pumps. This is what is known as the 5th generation DH networks, also known as District Energy Networks (DEN) or District Heating and Cooling (DHC). Besides the higher energy and exergy efficiency,

which reduce the operating costs, this technology also reduces the upfront costs. Given the lower distribution temperature, in fact, the pipes require less insulation, as well as they can be placed in shallower depth in the ground.

This technology has appeared in Switzerland in 2007, and it's mostly known as *anergy network*, or in german *Anergienetz*. To the authors knowledge, there are seven such systems operating by the end of the year 2018 [8]. A summary of a selection of four of them is shown in Table 1, while more detailed information can be found in the Appendix A [8].

Table 1: District energy systems in Switzerland; *n/a*: not available

	Anergienetz ETH Hönggerberg	Suurstoffi- Areal	Anergienetz Friesenberg (FGZ)	Genève-Lac- Nations (GLN)
Location	Zürich	Rotkreuz	Zürich	Genève
Year of construction	2012 - 2026	2010 - 2020	2011-2050	2008 - 2016
Energy Ref. Area [m²]	475'000	172'421	185'000	840'000
Inst. Heating capacity [kW]	8'000	6'732	3'930	4'300
Heating demand [MWh/a]	28'450	10'619	35'000	5'000
Inst. Cooling capacity [kW]	6'000	2'327	3'500	16'200
Cooling demand [MWh/a]	26'200	2'364	80'000	20'000
Distribution fluid	water	water	water	water
Heat source	Laboratories waste heat +HP	Waste heat buildings + PVT (solar th.) +HP	Waste heat data center+HP	Lake water +HP
Heat storage	Geothermal well field (431 at 200m)	Geothermal well field (215 at 150 m, 180 at 280m)	Geothermal well field (332 at 250m)	None
T of heating pipe	24 °C - 8 °C	25 °C - 8 °C	28 °C - 8 °C	17 °C - 5 °C
T of cooling pipe	4 °C - 20 °C	4 °C - 17 °C	4 °C -24 °C	5 °C - 12 °C
Tot. investments [MillionCHF]	37	n/a	42.5	33
Tot. COP of heating (incl. Pumps...)	5.8	2.7	4.1	6.5

All the anergy networks presented in Table 1 still base on water as a working fluid. Therefore, they work on sensible heat, which means that a heat exchange is bound to a variation in the fluids temperature. The challenge of these systems is given by the flow rate that is necessary to limit the temperature difference between the inlet and the return temperature of the network. Thus, it could be very interesting to use refrigerants, instead of water, that enable to work with latent heat instead, which means collecting and distributing heat through the condensation, or the evaporation, of the refrigerant. This poses some additional technological challenges, but has also very clear advantages, as it will be shown in the next chapters.

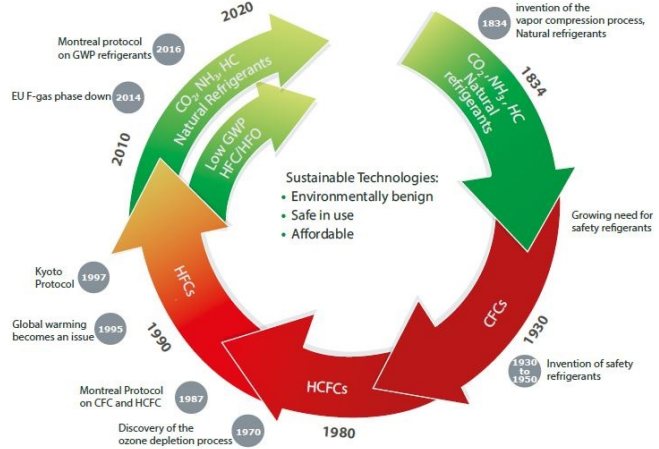


Figure 4: The historical cycle of refrigerants Source: [9]

The choice of the refrigerant strongly depends on the application. In function of the operating conditions, three main criteria are evaluated: affordability, safety and environmental impact. A summary of the history of refrigerants is shown in Figure 4. The Montreal protocol, signed in 1987, designed the phase out of HCFC and CFCs, in order to prevent ozone layer depletion. This boosted the use of HFCs, as a replacement. However, not far later, it has been realized that despite being less damaging to the ozone layer, they were powerful greenhouse gases. Since 2013, a federal ordinance also strongly restricted the use of these last ones in Switzerland [10]. Also Europe planned the phase-out of HFC in 2014 [11]. This means that today the choice of refrigerants is essentially limited to natural refrigerants - as for example CO₂ (R744), ammonia (R717) or propane (R290) - and the new environmentally friendly HFOs - as for example the fluorinated propane isomer R1234yf.

The choice of CO₂ as a refrigerant relies, besides its thermodynamic properties, on the following arguments [12]:

- it is very abundant in the environment and is also waste of a multitude of industrial processes
- it is harmless to the biosphere
- it is non-flammable and non-toxic
- it is an inert gas

In fact, according to Danfoss [9], CO₂ will dominate industrial refrigeration, together with ammonia. Already today, this technology is widely used. For instance Migros, Switzerland's largest retail company, opened its first supermarket to use CO₂, in a low-temperature subcritical system, in 2002. By today, 411 of the 700 supermarkets in Migros's portfolio are equipped with transcritical CO₂ systems [13].

2.3 CO₂ district energy network

2.3.1 The technology

Weber and Favrat [6] compared the performance of a DEN using subcritical CO₂, HFO R1234yf and water. They were able to show that the CO₂ network performs best, and has the biggest potential for DEN systems [14]. As explained above, a refrigerant based DEN technology allows to store and transfer heat through the latent heat of vaporization of the refrigerant. The operating pressure is chosen in order to obtain the desired temperature in the system. That temperature is

selected to be as high as possible to represent a good heat source for the decentralized heating heat pumps - resulting in good COP values -, while still allowing free cooling - avoiding the installation of compression chillers, and thus drastically reduce electricity consumption for space cooling.

The network consists of one saturated liquid pipe and of one saturated vapor pipe, both in a saturated temperature range from 12 to 18 °C [15]. The working principle is shown in Figure 5. Heating users can extract heat from the network through condensation of the refrigerant, taken from the vapour pipe. Respectively, cooling users take refrigerant from the liquid pipe and evacuate heat by evaporating it. The heat exchanges between the network and the users occur through condenser-evaporators heat exchangers, which keep the different refrigerant loops isolated [14]. The synergy between simultaneous heating and cooling users allows the recovery of waste heat. Most of the time, the required heating and cooling capacity will not be equal, which means that there is the need for a centralized balancing power. Indeed, a central plant is responsible to balance the overall network, by exchanging heat with the environment. For instance, a ground/water or a water/water heat pump can be used for this purpose.

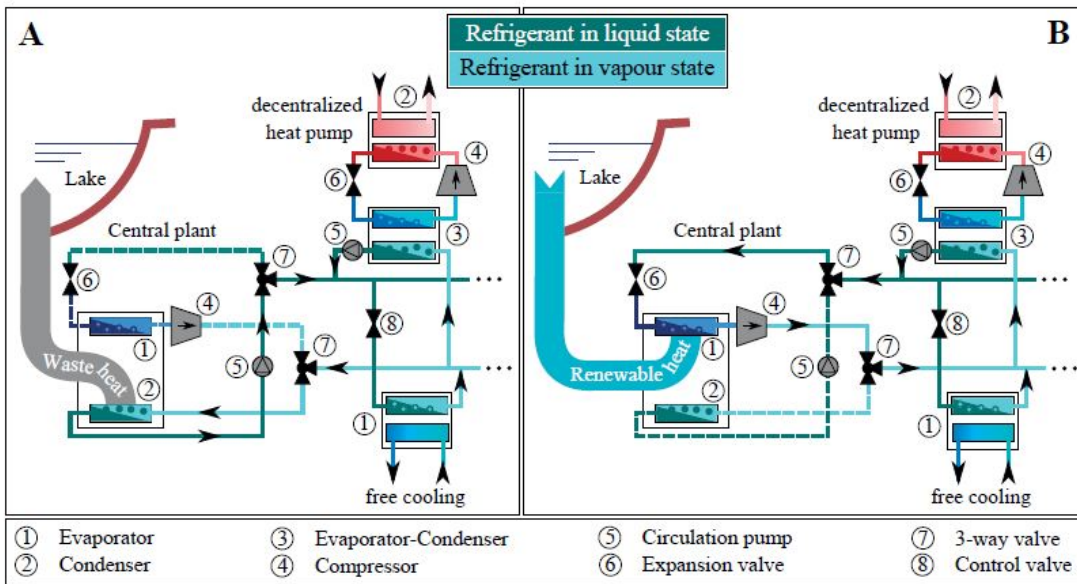


Figure 5: Schematics of a refrigerant based district energy network. Part A represents its net cooling operation, and part B its net heating operation. Source: [14]

One of the big advantages of this technology, with respect to water based DEN, is the pipes sizing. In fact, given the fact that it works on pressure maintenance instead of a fluid flow, no return pipe is necessary, which results in a slightly shorter total length of installed pipes. Moreover, due to the higher energy density of latent heat, the pipes diameters are drastically reduced. Henchoz et al. [14] compared three different working fluid on the same study case, showing that, while CO₂ needs pipes of only 280/330mm (liquid/vapor), R123yf would need 270/700mm (liquid/vapor) and water 625/625mm (liquid/liquid). Given the low operating temperatures, there are much lower requirements for pipes insulation. While water pipes need to be buried deep enough to prevent damage due to water freezing, in case part of the network had to be stopped during winter, CO₂ does not freeze and thus does not require a minimum freeze-safe depth. Henchoz et al. have even imagined installing the pipes inside a sidewalk module, which would drastically simplify maintenance and inspection. Given the smaller diameter, it would also be possible to retrofit an old, high temperature district heating network, by placing the CO₂ pipes inside the old water pipes. All the above mentioned advantages of using CO₂, result in lower upfront costs.

The main drawback of this technology is the high operating pressure - about 50 bars - and the safety concerns that could derive from the large amount of CO₂ that could escape in case of

a major leakage. Nevertheless, as described in 2.2, CO₂ refrigeration networks are already widely used in supermarkets, and the technology is considered as safe.

2.3.2 Performance

Henchoz et al.[14] performed an analysis of the potential application of a CO₂ based DEN in a district in the city of Geneva. A map of the district, called "Rues basses", is shown in Figure 6.

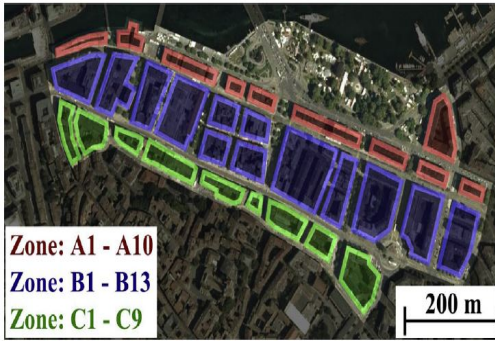


Figure 6: Representation of the the studied area and of its subdivision into 32 zones. Source: [14]

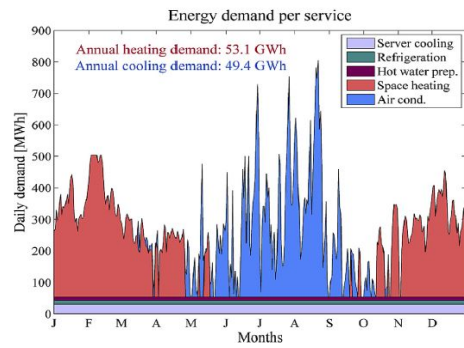


Figure 7: Energy demand for the area studied over the year 2012. Source: [14]

Table 2 shows the distribution of building affectations - which is important to determine the energy consumption - in the studied area. The total ERA is 687'800 m².

Table 2: Distribution of the energy reference area for the different zones and building affectations

Zones	Commercial [m ² ERA]	Offices [m ² ERA]	Residential [m ² ERA]
A1 - A10	20'700	89'200	17'700
B1 - B13	97'000	260'700	61'600
C1 - C9	40'400	62'600	48'100
Relative share	23%	60%	17%

The energy demand of heating (53.1GWh/yr) and cooling (49.4GWh/yr) in the studied area is shown in Figure 7. Throughout the year, the district presents nearly the same heating demand as for cooling, but they happen in different seasons.

The proposed CO₂ based DEN is balanced by a central plant - a heat pump - that exchanges heat with the nearby lake. In order to benchmark the results, this technology has been compared to a traditional heating and cooling system, based on oil boilers and cooled compression chillers.

The results are remarkable. In fact, the CO₂ based DEN shows a final energy consumption of 10,968 MWh of electricity, which corresponds to a reduction of 84.4 %, with respect to the reference scenario. Its exergy efficiency situates between 40-45%.

2.3.3 Integration in smart energy system

The integration of high shares of renewable energy represents an important challenge. In fact, it requires a lot of slack to handle the volatile nature of renewable energy sources like wind or sun. On one side, this slack will be mainly given through a smart control of the electricity grid on multiple levels. It starts from the demand side management (DSM) inside households, through optimization at district level, up to a national and international control. These decentralized grids,

or grid controls, are called *smart grids*.

With the vast success of heat pumps throughout the last decade, the control of electricity grids is more and more interconnected with the production of heat. This further complexifies the system by adding a level of constraints, but it also opens new levels of control. Indeed, if well designed, a DEN offers an additional level of slack that can be used in combination with the smart grid, multiplying control power. The CO₂ DEN offers several possibilities to shift the loads, relieving the grid.

On the one hand, it simplifies the deployment of a smart control of the heat pumps, which can strongly contribute in the DSM. The decentralized heat pumps can make use of a buildings thermal inertia to adapt electricity use to energy availability. CO₂ vapor and liquid storage can act as a buffer, enabling load-shifting also for the central plant of the DEN. Sizing of these storage capacities will determine the possible time-span that the shift can achieve. Given the low distribution temperature, this approach also facilitates the storing of heat, as for example in a geothermal field.

On the other hand, the use of CO₂ as a refrigerant for the network could improve the integration of a power to gas (PtG) system. Indeed, one big challenge in the future, especially in higher latitudes, where seasonal variation are consistent, is to ensure energy supply during winter season, when, due to shorter and weaker solar irradiation, PV panels produce less. It is thus important to find a way to store the excess of renewable energy production during the summer, in order to use it in the winter. One solution to do that is PtG, which defines the process of transforming electrical power to a gas, like methane, which is easy to store. To do so, electricity is used to produce hydrogen, which can be combined with CO₂ to form Methane, in a process called methanation. Methane can be used during winter to produce electricity and heat, in a combined heat and power plant (CHP), as for example a SOFC, a gas turbine, or a combination of them. For this reason, PtG is widely studied across Europe and many pilot plants have already been built [16].

Suci et al. [15] studied the synergy between a CO₂ based DEN, decentralized PV and such a PtG system. The CO₂ network could be used to store the carbon dioxide, which is captured from CHPs or industrial processes during winter, needed for methanization. At the same time, the DEN can directly use and dispatch the heat produced from the CHPs. In their work, they analyzed the PV area, and thus the investment, required to achieve a completely autonomous energy system, for different European climatic zones. The results showed that decarbonized autonomous energy systems based on DENs and PtG technologies are possible, along with a very broad deployment of solar energy. It is also shown that the payback time of such a system is between 11 and 14 years, which is relatively low compared to its life time.

2.4 Direct-expansion ground source heat pump

For heat pumps based systems, sourcing heat from the soil, instead of from the ambient air, is a very interesting solution at central European latitudes, especially, as it has been seen, for integration of a 5th generation DEN, since it improves heating and cooling COPs, and, to a certain extent, it allows heat storage. In traditional Ground-Source Heat Pumps (GSHP), the heat pump and the ground are connected by means of a closed loop, using water, or a water solution. This system, called the secondary loop GSHP (SL-GSHP), is shown on the right side of Figure 8. However, it has been proved [17, 18] that the system efficiency can be improved, by directly expanding the refrigerant into the ground, avoiding the secondary water loop. Shown on the left side of Figure 8, this system is called Direct Expansion GSHP (DX-GSHP).

So far, this technology is not so widely spread, mostly because of a more demanding system design and because of the risk of environmental pollution, when non-natural refrigerants are used. Indeed, literature about DX-GSHP is still scarce, especially for CO₂ as a refrigerant. There are only few numerical CO₂-DX-GSHP studies [19, 20, 21, 22], which are not yet sufficient to obtain a scientific appreciation of the technology. Nevertheless several prototypes and experimental set-ups have been built and analyzed [23, 24, 18], showing that higher efficiencies can be reached through DX, with respect to a SL.

One of the main reasons for this efficiency gain is the elimination of the temperature lift of the water loop, which is replaced by a constant temperature phase-change, as well as the elimination

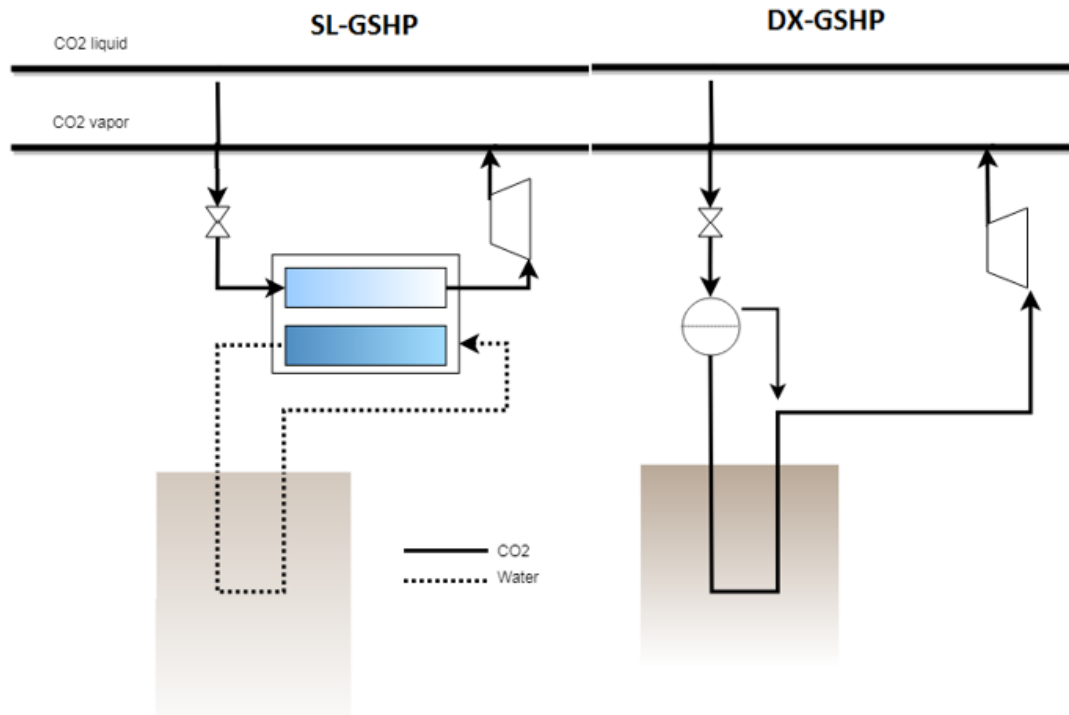


Figure 8: A simplified schematics of the two GSHP technologies

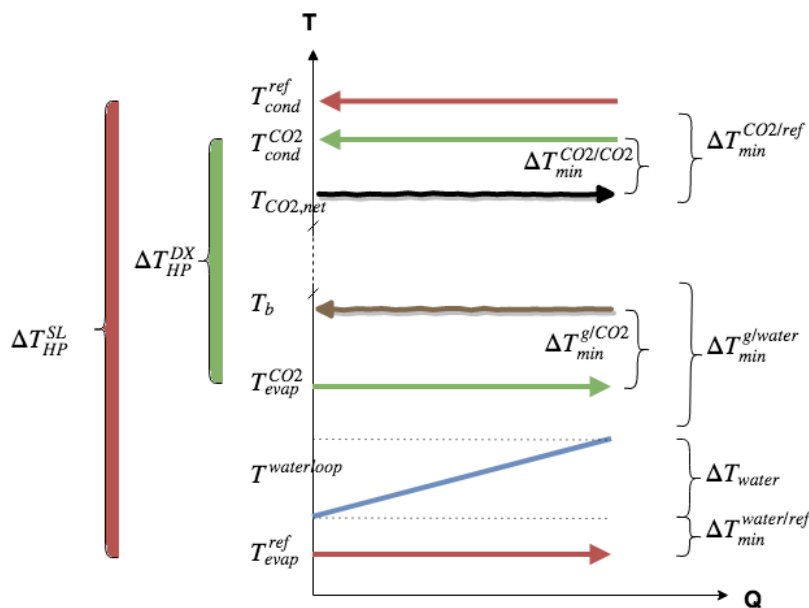


Figure 9: Schematic representation of heat exchanges and minimum approach temperatures for the central plant HP, comparing SL- and DX-GSHP

of the minimum approach temperature necessary to exchange heat between the SL and the heat pump, as shown in Figure 9. The resulting temperature rise for the DX-GSHP ΔT_{HP}^{DX} is much lower than ΔT_{HP}^{SL} for the SL-GSHP, leads to a higher COP for the heat pump. Moreover, CO₂ presents a higher heat transfer coefficient, which again allows to either reduce the minimum approach temperature, or extract a higher power with respect to an equal exchange surface. The minimum approach temperature has to be determined in function of the thermal permeability of soil and is correlated to the length and total surface of the geothermal probes, as well as the refrigerant flow rate.

3 Methodology

3.1 Energy demand - Typical days

The energy demand profile for space heating and cooling is calculated as a linear function of the temperature difference with the ambient temperature [25]. Specific energy requirements per square meter in function of the typology of the building are taken from SIA (Schweizerischer Ingenieur- und Architektenverein) standards [26].

The optimization of an energy system is commonly performed over the time span of one year, in order to account for the different seasons. However, this requires a very long computing time, given the high number of time steps. Thus, it is common to group similar days, according to a set of parameters as for example temperature or irradiation, into so called typical days. The days can be clustered in different ways. It can be chosen to compute an average day for each month or some machine learning clustering algorithm - as for example K-means, DBSCAN or GMM - can be used to group the days into the desired number of clusters. The resulting typical days correspond to a period p , with a number of times t , as explained in section 3.7. In order to account for the data compression, a value called *occurrence* indicates how many times a given typical day occurs, i.e. how many times a given period occurs.

Two additional days with the two opposite extreme temperature conditions are added to the typical days, in order for the model to account for them in the equipment sizing. To avoid a bias of the operation results, those days are set with an occurrence of zero.

3.2 Geothermal wells

The most important parameter in geothermal wells is the soil temperature, which is normally constant throughout the year. In fact, only the first 10 meters are influenced by the temperature of the air [27]. Moreover, the temperature increases with depth. According to the SIA norm SIA384 [28], the mean temperature in a geothermal well can be calculated by:

$$T_{g,mean} = T_{g,sup} + \frac{L_w \cdot \nabla T_g}{2} \quad (1)$$

where $T_{g,sup}$ is the ground temperature at the surface, L_w is the length of the well and ∇T_g is the temperature gradient of the soil.

The energy demand of the circulating pumps is assumed to be negligible.

3.3 Investment cost function

To calculate the investment cost for a given technology, it is possible to interpolate data from available products on the market. However, it is also possible to evaluate it with help of a cost function [29].

First, it is necessary to calculate the cost of purchase of the unit, in function of its size, given by the sizing parameter, which can be the electrical power E , the delivered heat Q or the area of a heat exchanger A .

$$C_{pex} = \frac{I_t}{I_{t,ref}} \cdot 10^{(k_{1,ex} + k_{2,ex} \cdot \log(E/Q/A))} \quad (2)$$

Through a factor called *Bare Module Factor*, the accessory costs of transport, installation, connection are included in the calculation, obtaining the total investment costs

$$CBM_{ex} = C_{pex} \cdot FBM_{ex} \cdot e \quad (3)$$

where e is the currency ration from USD to CHF. The annuities are calculated with the annuitization factor (af), where n is the assumed lifetime of the equipment in years, and i the interest rate.

$$IC_{yearly,ex} = CBM_{ex} \cdot af \quad af = \frac{i \cdot (1+i)^n}{(1+i)^n - 1} \quad (4)$$

This investment cost function is not a linear function. However, as described in Section 3.7, to solve the MILP it is necessary to provide a set of linear parameters that approximate the function. These are found by linearizing the investment cost function around the reference value, defined in the range of application. This was done with help of a matlab code, using *polyfit* and *polyval* functions. Figure 10 shows the linearized function with the according cost parameters.

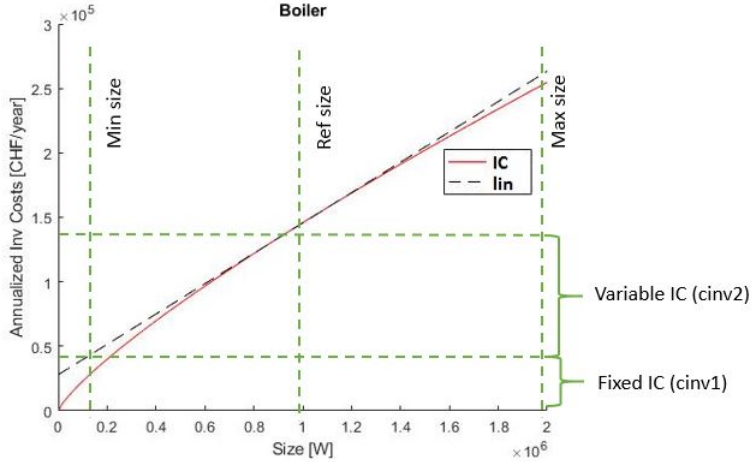


Figure 10: Linearization of investment cost function

3.4 Minimum approach temperature

The critical sizing parameter for a heat exchanger is the minimum approach temperature ΔT_{min} , which corresponds to the smallest temperature difference in the heat exchanger between the hot and the cold stream, as shown in Figure 11. This value is strongly dependent on the heat exchanger area A_{ex} and the heat transfer coefficients h of the exchanging fluids.

$$A_{ex} = \frac{Q_{ex}}{U \cdot LMTD} \quad (5)$$

$$LMTD = \frac{(T_{Hot,in} - T_{cold,out}) - (T_{Hot,out} - T_{cold,in})}{\log \left(\frac{T_{Hot,in} - T_{cold,out}}{T_{Hot,out} - T_{cold,in}} \right)} \quad (6)$$

$$T_{Hot,in} = T_{cold,out} + \Delta T_{min} \quad (7)$$

where $LMTD$ is the logarithmic mean temperature difference and T are the inlet and outlet temperatures of the hot and cold streams, as shown in Figure 11. The overall heat transfer coefficient [30] is given by:

$$U = \frac{1}{\frac{1}{h_{(hot)}} + \frac{1}{h_{(cold)}}} \quad (8)$$

where $h_{(hot)}$ and $h_{(cold)}$ are the heat transfer coefficient of the hot and cold fluid.

The optimization is done by minimizing the total cost of the system dependent on the heat exchange, which include the investment and operating costs of the compressor, as well as the investment costs of the heat exchanger:

$$\min_{\Delta T_{min}} \{OC(\Delta T_{min}) + IC(\Delta T_{min})\} \quad (9)$$

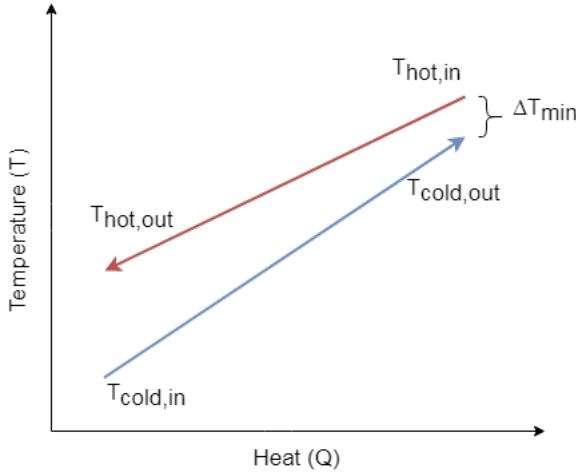


Figure 11: Minimum approach temperature in a counter-flow heat exchanger.

A bigger A_{ex} allows a smaller ΔT_{min} , which increases the investment costs of the heat exchanger. However, a smaller ΔT_{min} also reduces the temperature difference that the heat pump has to achieve in order to exchange heat, thus increasing its COP. This leads to a lower electricity consumption, i.e. lower operating costs, as well as to a lower investment cost of the compressor. An optimum can be found for each specific application.

Heat transfer coefficients used in this work are shown in Table 3. For R134yf, the heat transfer coefficient appears to be the same as for R134a [31], while for CO₂ (R744) experimental values are used [32, 33].

Table 3: Heat transfer coefficients found in literature

Fluid	Water	R134yf	R744
$h[W/(mK)]$	600	3000	7000

3.5 Exergy

The exergy of an energy transfer is defined as the maximum amount of work that can be extracted from it, through reversible transformations that exchange with the environment. Thus the calculation of exergy losses is a very interesting indicator to analyze a given process or system, since it expresses the quality and the efficiency with which the system operates, with respect to the maximum possible. Therefore these values are always lower than 100 %.

The exergy value, i.e. the maximum work that can be extracted from an energy transfer, or the minimum work needed to satisfy an energy demand, is derived from the first two thermodynamic principles, and is given by the following formula [14]:

$$\dot{E}_{max}^- = \sum_i \dot{Q}_i^+ \left(1 - \frac{T_a}{T_i}\right) + \sum_r \dot{M}_r^+ (h_r - T_a s_r) \quad (10)$$

The exergy losses are thus given by the difference between the exergy value and the energy furnished to the system:

$$\dot{L} = \dot{E}_{max}^- - \sum_j \dot{E}_j^- \geq 0 \quad (11)$$

$$\dot{L} = (1 - \eta_{exergy}) \dot{E}_{max}^- \quad (12)$$

In the case of a heat pump based energy system, the exergy is given by:

$$\eta_{exergy} = \frac{\dot{E}q_{cold,a} + \dot{E}q_{hot,r}}{\dot{E}_{el}^+} \quad (13)$$

$$\dot{L} = (1 - \eta_{exergy})\dot{E}_{el}^+ \quad (14)$$

where $\dot{E}q_{hot,r}$ and $\dot{E}q_{cold,a}$ are the exergy value of respectively the hot streams below (r) and the cold streams above (a) the ambient temperature; these correspond to the exergy value of the heating and cooling demand. \dot{E}_{el}^+ is the electricity consumed by the defined system, which corresponds to the energy furnished to the system in order to satisfy the demand.

3.6 Energy technology models

The models for the energy technologies are adapted from an existing source code [34], as explained in detail, in this chapter.

3.6.1 Heat pump - Carnot cycle

Heat pumps can be modeled in a simple way, using the principle of the Carnot cycle, with help of the following equations:

$$\dot{E}_{compressor} = \frac{\dot{Q}_{cond}}{COP_{real}} = \frac{\dot{Q}_{cond}}{\eta_{COP} \cdot COP_{theoretical}} \quad (15)$$

$$COP_{theoretical,heating} = \frac{T_h}{T_h - T_c} \quad COP_{theoretical,cooling} = \frac{T_c}{T_h - T_c} \quad (16)$$

where \dot{Q}_{cond} is the heat delivered and \dot{Q}_{evap} the heat sourced by the heat pump. η_{COP} is an experimentally defined efficiency to account for irreversibility of the cycle, i.e. to give the ratio between the theoretical and the real COP. The values used in this work are shown in Table 4, calculated by Girardin et al.[25], based on values obtained from a heat pump certification center [35].

Table 4: Theoretical efficiency factor for COP

Type	Size	η_{COP}
Air/Water	Decentralized	0.34
CO ₂ /Water	Decentralized	0.43
Ground/Water	Decentralized	0.43
Ground/Water	Centralized	0.55
Water/Water	Centralized	0.55

3.6.2 Heat pump - Thermodynamic cycle

A more accurate model of the heat pumps, that is able to correctly represent and calculate the operating cycles and conditions, is achieved by modeling its thermodynamic cycle [36], represented in Figure 12:

1 - 2 : Expansion to low pressure level

2 - 3 : Evaporation by cooling down the heat source

3 - 3sh : Superheating in evaporator

3sh - 4 : Compression to high pressure level

4 - 1 : Condensation of refrigerant, delivering heat

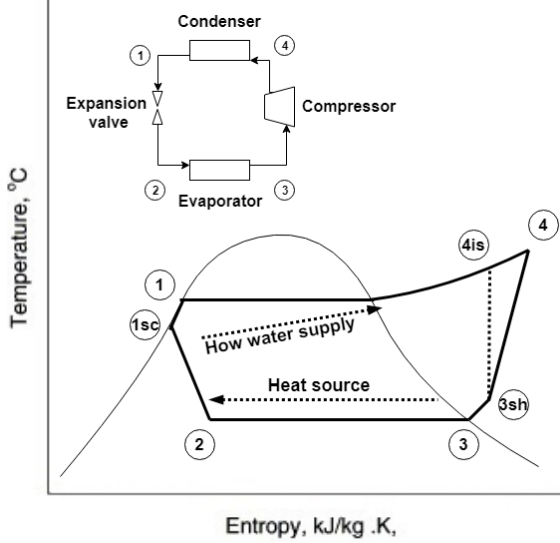


Figure 12: Temperature–entropy diagram of a R134yf based heat pump system.

The compressor is a crucial component for the design of a heat pump, since it has the largest share of impact on the energy efficiency. To calculate its efficiency, the model of Hu et al.[30] has been used. The shaft power can be computed in function of the isentropic efficiency (η_{is}) by:

$$W_{shaft} = \frac{\dot{m}(h_{d,is} - h_s)}{\eta_{is}} \quad (17)$$

where $h_{d,is}$ is the isentropic discharge enthalpy and h_d is the suction enthalpy. The compressors input power is expressed in function of its mechanical efficiency (η_{mech}) by:

$$E_{comp} = \frac{W_{shaft}}{\eta_{mech}} \quad (18)$$

The numerical values of those efficiencies are strongly dependent on the ratio between the pressure of discharge P_d and the pressure of suction P_s of the compressor. They can be computed inside the model with help of the relations obtained by Li et al.[37]:

$$\eta_{mech} = 0.85 \quad (19)$$

$$\eta_{is} = 0.874 - 0.0134 \cdot \left(\frac{P_d}{P_s}\right) \quad (20)$$

$$(21)$$

The expansion of the refrigerant in the expansion valve is assumed to be isenthalpic.

Thus, the procedure to evaluate the operating conditions of the heat pump is the following:

1. calculate thermodynamic state in point (1) knowing the evaporation temperature T_{evap} and assuming saturated liquid
2. calculate thermodynamic state in (1sc) using same pressure as in (1), with $T = T_{evap} - \Delta T_{subcool}$
3. calculate thermodynamic state in point (3) knowing the evaporation temperature T_{cond} and assuming saturated vapor
4. calculate thermodynamic state in (3sh) using same pressure as in (3), with $T = T_{cond} + \Delta T_{superheat}$

5. calculate thermodynamic state in (2), assuming isenthalpic expansion of the valve, with $H_2 = H_{1sc}$ and P_3
6. calculate isentropic efficiency of compressor $\eta_{c,is}$, knowing the discharge pressure P_1 and the suction pressure P_3
7. calculate thermodynamic state in (4is), assuming an isentropic compression with S_{3sh} and P_1
8. calculate thermodynamic state in (4), accounting for the isentropic efficiency of the compressor $\eta_{c,is}$, using $H_4 = H_{3sh} + \frac{H_{4is} - H_{3sh}}{\eta_{c,is}}$, and P_{1sc} .

In Osmose, these values are calculated with help of *Coolprop*, which is an open-source database of fluid and humid air properties that allows to calculate operating conditions for a large number of fluids and refrigerants. Thanks to a *lua wrapper*, which is a *lua* module that provides an API to the external software, *Coolprop* is called inside Osmose.

The electrical power of the heat pump and its COP, are then calculated by:

$$E_{el} = \frac{m_{ref} \cdot (H_4 - H_{3sh})}{\eta_{mech}} \quad (22)$$

$$Q_{cond} = m_{ref} \cdot (H_4 - H_{1sc}) \quad (23)$$

$$COP = \frac{Q_{cond}}{E_{el}} \quad (24)$$

where m_{ref} is the massflow of refrigerant in the heat pump.

3.6.3 Heat pump - Supercritical CO₂

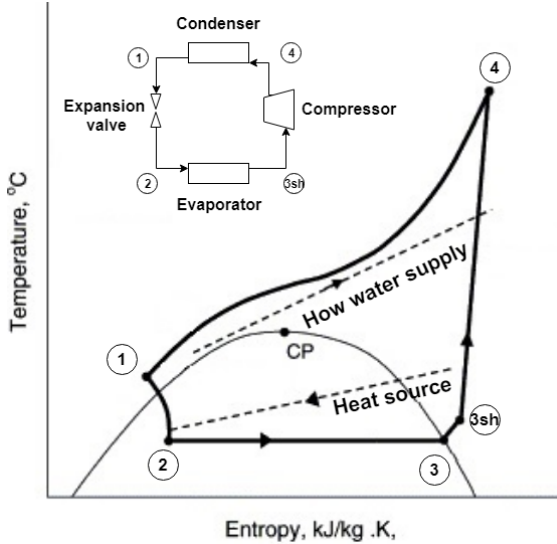


Figure 13: Temperature–entropy diagram of a trans-critical CO₂ heat pump system for a domestic hot water production. Source: [38]

In traditional heat pumps, the heat delivery occurs through condensation of the refrigerant, which happens at a fixed temperature. This originates high exergy losses, especially in processes where a high temperature lift is needed in the gas cooler. Some refrigerants have the particular property of having a very low critical point. Among others, a very interesting one is CO₂ – technically known as R744 –, which has a critical point at 74 bars and 31 °C[12]. As explained in Section 2.2, CO₂ is also a very interesting choice for environmental and financial reasons.

The supercritical cycle is shown in Figure 13, represented on the temperature-entropy diagram. The different steps of the process are explained hereafter:

1 - 2 : Expansion to low pressure level

2 - 3 : Evaporation by cooling down the heat source

3 - 3sh : Superheating in evaporator

3sh - 4 : Compression to transcritical pressure

4 - 1 : Gas cooling in transcritical area, to heat water

Note that, as there is no phase change, the heat exchanger is called gas cooler, instead of condenser.

Even though the technological development is slowly closing the gap, CO₂ compressors have lower isentropic efficiency and lower volumetric efficiency than subcritical ones [39]. This comes from the high irreversibility caused by the superheated vapor horn and the high throttling losses [40]. However, transcritical operation also allows heat to be exchanged on a varying temperature, and the heat pump can be designed to fit the heat demand stream, optimizing exergy efficiency. This is particularly interesting in exchanges that require high temperature lifts, as in the case of domestic hot water heaters. In fact, this can be seen in Figure 13, between point 4 and 1. For instance, Stene et al. show that COP for a CO₂ HP is lower if it is used in subcritical range - for Space Heating (SH) (35/30 °C) - than in supercritical range - Domestic Hot Water (DHW) (10/60 °C) -, despite the much higher temperature difference. They also show that the resulting COP for DHW application outperforms conventional HPs [41].

For the transcritical CO₂ heat pump, the numerical values of the compressor efficiencies computed with help of the relations obtained by Wang et al [42]:

$$\eta_{mech} = 0.64107 + 0.07487 \cdot \left(\frac{P_d}{P_s} \right) \quad (25)$$

$$\eta_{is} = 0.8014 - 0.04842 \cdot \left(\frac{P_d}{P_s} \right) \quad (26)$$

(27)

The procedure to evaluate the operating conditions of the heat pump is the following:

1. calculate thermodynamic state in (1) with help of the temperature at the outlet of the condenser $T = T_{cond,out} = 15.5^\circ\text{C}$, optimized for this specific cycle by Henchoz et al.[43], and the pressure $P_{cond,out} = 84.9\text{bar}$, optimized to satisfy the required inlet temperature of the condenser
2. calculate thermodynamic state in point (3) knowing the evaporation temperature T_{evap} and assuming saturated liquid
3. calculate isentropic efficiency of compressor $\eta_{c,is}$, knowing the discharge pressure P_1 and the suction pressure P_3
4. calculate thermodynamic state in (4is), assuming an isentropic compression with S_{3sh} and P_1
5. calculate thermodynamic state in (4), accounting for the isentropic efficiency of the compressor $\eta_{c,is}$, using $H_4 = H_{3sh} + \frac{H_{4is} - H_{3sh}}{\eta_{c,is}}$, and $P_{cond,out}$.
6. calculate thermodynamic state in (2), assuming isenthalpic expansion of the valve, with $H_2 = H_1$ and P_3

The equations to calculate electrical power of the heat pump and its COP, are the same as in Section 3.6.2.

3.6.4 Outdoor condensing unit

An outdoor condensing unit is an equipment used to cool down a hot stream through the ambient air. This is used in air-cooled air conditioning or refrigeration systems, to evacuate the heat into the environment. It consists of a set of fans that blow the air through a heat exchanger. These fans originate a parasitic power consumption [14] that can be calculated with help of the following equation:

$$\dot{E}_{fans} = \frac{0.605 \cdot \dot{Q}_{cond}}{(\Delta T_{air} + \Delta T_{min}^{ref/air})^{0.9937}} \quad (28)$$

where \dot{Q}_{cond} is the heat to be dissipated in the environment by the condenser.

3.6.5 Geo-cooling

Geo-cooling is the use of fresh temperatures of the ground for space cooling. This happens by simply circulating a fluid between the buildings, where the heat is extracted, and the geothermal wells, where heat is released into the ground. In practice, this happens by bypassing the heat pumps and making the water of the secondary loop (geothermal loop) directly exchange with the heating water loop. Investment costs are, thus, limited to an additional heat exchanger.

The energy needed for circulation pumps is assumed to be negligible.

3.6.6 PV

The efficiency of the PV panels η_{PV} is given by the following equation [44]:

$$\eta_{PV} = \eta_{ref} - \eta_{var}(T_{panel} - T_{ref}) \quad (29)$$

where η_{ref} and η_{var} are respectively the fixed efficiency and the temperature dependent efficiency. The temperature of the panel T_{panel} is calculated by means of:

$$T_{panel} = \frac{U_{glass} \cdot T_{amb} + GI \cdot f_{glass} - \eta_{ref} - \eta_{var} \cdot T_{ref}}{U_{glass} - \eta_{var} \cdot GI} \quad (30)$$

where U_{glass} is the thermal transmittance of the front glass, f_{glass} is the light transmittance of the front glass and GI is the global irradiation. Thus, the produced energy is given by:

$$E = GI \cdot A_{PV} \cdot \eta_{PV} \quad (31)$$

The area of installed PV A_{PV} is expressed in function of the total roof area of the buildings A_{roof} :

$$A_{PV} = A_{roof} \cdot f_{area} \quad (32)$$

The area factor f_{area} for flat roofs - which accounts for the optimal distance between the panels, obstacles and margins - is assumed to be $\frac{1}{4}$.

3.6.7 Network

The length is calculated, according to a simplified method [25]:

$$L = 2(n_b - 1)K \sqrt{\frac{S}{n_b}} \quad (33)$$

with S being the land area, n_b the number of buildings. The constant K is chosen at 0.5. And diameter of the pipes:

$$d = \sqrt{\frac{4 \cdot \dot{m}}{\pi v_s \rho}} \quad (34)$$

assuming a sizing velocity v_s of 3 m/s, calculated to be the maximum velocity of liquid flow in pipelines of 300-500 mm diameter that avoids rapid aging caused by abrasion, cavitation and fatigue [43]. The investment costs are calculated accordingly:

$$C = \sum_{k=1}^{n_b} \frac{L}{n_b} (c_1 d \sqrt{n_b + 1 - k} + c_2) \quad (35)$$

where $c_1 = 5670$ and $c_2 = 613$.

Operating temperature is assumed to be 13 °C for the liquid pipe and 15 °C for the vapor pipe [34].

The pressure losses, and thus the energy needed for the maintaining of the pressure, are assumed to be negligible.

3.7 MILP optimization and Osmose

Mixed integer linear programming (MILP) is a mathematical optimization, in which some variables are restricted to be integers, while other are discrete. A MILP model can be written with AMPL (A Mathematical Programming Language), which is a modeling language specifically designed to describe and solve optimization problems. Once defined the model, this is passed to a solver, as for example Gurobi or GLPK, which solves the given problem.

Osmose is a platform developed at IPESE for the study and the design of complex integrated energy systems. Its aim is to allow the user to model and compute an optimization problem using the same platform, which would normally require to access and transfer data between several programs. The coding language is *lua*.

Osmose allows to define a model for the different energy conversion technologies that want to be analyzed. It will then prepare the necessary files for the optimization of the energy system that will be handed over to AMPL. After the solving is complete, the results sent back to Osmose, allowing to post-process the data to run sensitivity analysis, multi-objective optimizations or simply calculate performance indicators.

In first place, energy technologies have to be defined, with its set of equations that determine the supply and the demand of the unit. Moreover it is necessary to furnish the following cost parameters:

- c^{inv1} : fixed part of the IC, given in [CHF/year]. This can be found in Figure 10 in Section 3.3;
- c^{inv2} : variable part of the IC, given in [CHF/year]. This can be found in Figure 10 in Section 3.3;
- c^{op1} : fixed part of the OC, which corresponds to maintenance and service costs.
- c^{op2} : variable part of the OC. This is the operating cost resulting from the system optimization, also in [CHF/h].

The sizing of the energy conversion technologies is constrained with the following equations [15]:

$$f_{u,t} \leq f_u \quad \forall u \in U, \forall t \in T \quad (36)$$

$$f_u^{min} \cdot y_u \leq f_u \leq f_u^{max} \cdot y_u \quad \forall u \in U \quad (37)$$

$$(38)$$

where U is the set of units, and T is the set of operating times.

For *process units* - i.e. the subset of units U with a defined sizing, as for example the units in the industrial production line of a product - $y_u = f_u^{min} = f_u^{max} = 1$. In a residential district only

the houses, which are defining the energy demand, are considered as *process units*.

The total cost of the system is given by:

$$\sum_u^U \left[\sum_{t=1}^T (c_u^{inv1} \cdot y_{u,t} + c_u^{inv2} \cdot f_{u,t} + c_u^{op1} \cdot y_{u,t} + c_u^{op2} \cdot f_{u,t}) \cdot t_t^{op} \right] \quad (39)$$

$$(40)$$

A set of equations, called heat cascade, makes sure that heat is always transferred from a higher temperature to a lower one, also considering the respective minimum approach temperature for each stream.

$$\sum_u^U f_{u,t} \cdot \dot{Q}_{u,t,k} + \dot{R}_{t,k+1} - \dot{R}_{t,k} = 0 \quad \forall k \in K, \forall t \in T \quad (41)$$

$$\dot{R}_{t,k} \geq 0 \quad \forall k \in K, \forall t \in T \quad (42)$$

$$\dot{R}_{t,1} = \dot{R}_{t,k+1} = 0 \quad \forall t \in T \quad (43)$$

$$(44)$$

where K is the set of temperature intervals.

The demand $\dot{m}_{r,u,t}^+$ and the supply $\dot{m}_{r,u,t}^-$ of resource $r \in R$ of each unit $u \in U$ is computed:

$$\dot{M}_{r,u,t}^- = \dot{m}_{r,u,t}^- \cdot f_{u,t} \quad \forall r \in R, \forall u \in U, \forall t \in T \quad (45)$$

$$\dot{M}_{r,u,t}^+ = \dot{m}_{r,u,t}^+ \cdot f_{u,t} \quad \forall r \in R, \forall u \in U, \forall t \in T \quad (46)$$

$$(47)$$

where R is the set of resources. The balance of each resource has to be respected:

$$\sum_u^U \dot{M}_{r,u,t}^- = \dot{M}_{r,u,t}^+ \quad \forall r \in R, \forall t \in T \quad (48)$$

Electricity is also balanced:

$$\dot{E}l_{houses}^+ + \dot{E}l_{heating}^+ + \dot{E}l_{cooling}^+ + \dot{E}l_{grid}^+ = \dot{E}l_{PV}^- + \dot{E}l_{grid}^- \quad (49)$$

The objective function defines which parameters have to be maximized or minimized during the optimization process. It is common to choose to minimize either the operating, the investment costs or a combination of them. However, other parameters, as for example the amount of carbon emissions, can be considered.

4 Application

4.1 Case-study Eglantine

In the framework of the collaboration between Romande Energie and IPESE, a case study shall bring a concrete numerical case study into the discussion. For this, Romande Energie has chosen a real life example of a district in the city of Morges. This district is in the planning phase, and Romande Energie had worked on it, in order to participate in the call for tender. This case study shall be fertile ground to discuss the CO₂ DEN technology and its role in the future energy systems in Switzerland and, more particularly, in the future plans of Romande Energie.

4.1.1 Context



Figure 14: Localization of the terrain, at the town scale. Source: [45]

The “Eglantine” is a terrain in the western part of the city of Morges, as shown in Figure 14. It is located in the proximity of key urban facilities, as well as the countryside. This terrain, which was partly used for agriculture, and partly covered by rich vegetation, belongs to the municipality, who is planning to use it for the urban expansion. The municipality had the vision of building a new district, which would be planned to be exemplary in the sustainable development. After many years of revising and fine-tuning the land-use plan and its vision for the future, in the beginning of 2016, the commune launched a call for tender for the planning of the different aspects of the district. The call for tender regarding the energy system was opened by Losinger Marazzi the 1st December 2017, with a due date the 31 January 2018. The contract with the winner, unknown to the author, has been signed in the end of March 2018.

The call for tender requires the development of a complete energy system, including thermal and electrical energy. Estimated data about the buildings is provided and can be found in Appendix B. Those are based on the following assumptions:

- All buildings are certificated Minergie 2017
- Space heating and hot water energy demand follow the SIA 380/1 and SIA 2031 norms
- Air ventilation is defined according to Minergie 2017 principles.
- Installed power values are calculated according to SIA 2024 norm

4.1.2 Available data

The district, which will host around 1'500 people, is composed of fourteen buildings, as shown in Appendix B, which account for a total energy reference area (ERA) of around $47'000m^2$. The details are shown in Table 5. According to the Minergie standard, the district will require about $1.40MWh/yr$ for SH and $0.95MWh/yr$ for DHW.

Table 5: Estimated energy demand in call for tender

Buildings	Energy Ref. Area (ERA)	Inhabitants	Space Heating (SH) MIINERGIE simple flux [m ²]	Hot Water (DHW) SIA 380/1 [kWh/yr]	TOTAL [kWh/yr]
14	46'350	1'498	1'401'559	948'958	2'350'521

The call for tender includes also information about the end use of the buildings, which is shown in Table 6. It can be seen that the buildings include, beside the residential use, also a small share of retail and restaurant services use, which are associated with different energy needs. Moreover, there is even a small indoor swimming pool, located in building one.

Table 6: Total estimated use of buildings in call for tender

Category	Housing [%]	Retail [%]	Restaurant services [%]	Indoor swimming pool [%]
Tot	97.08 %	1.63 %	0.78 %	0.51 %

The energy profile of the buildings is calculated according to Minergie standard, as well as the SIA norms. Given the annual energy demand for space heating and hot water, as shown in Table 5, the monthly profile is shown in Figure 15.

Some pre-studies have been commissioned by the land-owner, in order to give, on an indicative basis, the sizing of the energy system. These studies have been realized by external engineering firms and the results are contained in the call for tender. The studied parameters include the sizing for heat pumps, geothermal wells, as well as PV, and are shown in Table 7. They estimate a PV potential on the building roofs of $570kWp$, and the need for an installed heating power of $1'258kW$, using 77 geothermal wells of an average length of $271m$.

Table 7: Estimated sizing of energy system in call for tender

HP [kW]	PV [kWp]	Geothermal Nb. wells	Average Depth [m]
TOT 1'258	570	77	267

Detailed data from the call for tender can be found in the Appendix B.

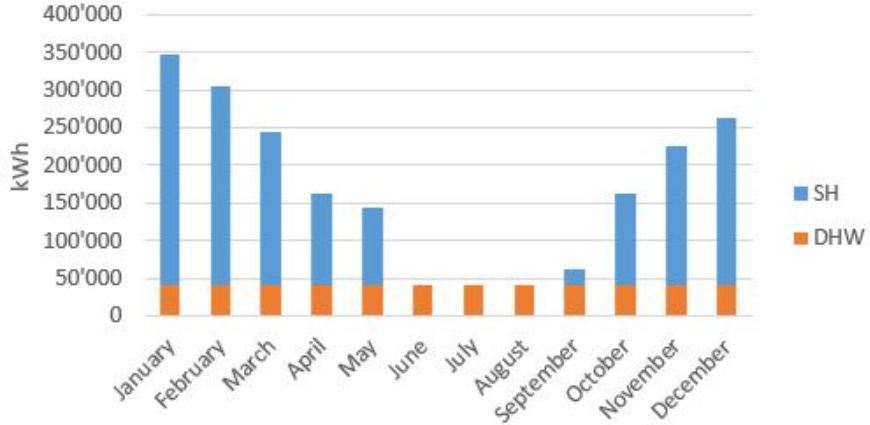


Figure 15: Annual energy distribution for space heating and hot water

4.1.3 Energy demand - Typical days

The profile of the energy demand is calculated as explained in Section 3.1. The used threshold temperature for heating is $T_{th}^{heat} = 14^\circ\text{C}$ and for cooling $T_{th}^{cool} = 18^\circ\text{C}$. The resulting energy demand, already multiplied by the number of occurrences for each time step, is shown in Figure 16.

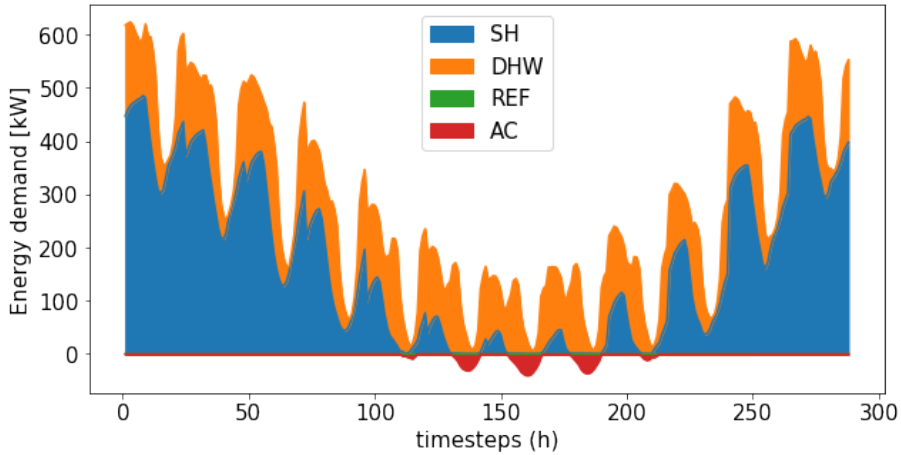


Figure 16: Total heating (+) and cooling (-) demand of the Eglantine district, for each time step

4.2 Heat sources

The heat pumps in a system can source heat from various sources. Its choice depends on the source temperatures and its investment costs. This chapter illustrates the different heat sources that have been considered in this work.

4.2.1 Stream

A small stream flows along the eastern boundary of the area, on which the Eglantine district is being built. However, the flow rate would not be sufficient to cover the heating/cooling demand, especially during the dry winter season [46]. For example, the lowest value has been reached in August 2004 with $0.017\text{m}^3/\text{s}$, and even in December 2005 the lowest daily flow was of $0.057\text{m}^3/\text{s}$. For this reason, the stream has been excluded from further analysis and has not been considered as a viable solution.

4.2.2 Lake

Lake water is commonly sourced at a depth of around 70 m, where a constant temperature of 7.5°C is found throughout the year. This water is led to the central pump through a water pipe. The massflow of the water is calculated in order to satisfy a drop/rise in the water stream of $\Delta T_{water} = 4^\circ\text{C}$.

The cost function is calculated as for the CO₂ pipes (see Section 3.6.7), considering the needed diameter to satisfy the heating/cooling demand, which depend on the different heat capacity and massflow of the water. The length of the pipes, which is measured on a GIS software, is of 1'500 m.

4.2.3 Geothermal wells

The average temperature of a geothermal well is calculated according to Section 3.2. The temperature gradient in the lemanic region is found in experimental data from Geneva canton [47]: $\nabla T_g = 0.03[\text{K}/\text{m}]$ (see Figure 48 in Appendix D). This value also corresponds to the average gradient found in the Swiss plateau [28].

The average surface temperature depends mainly on the latitude and on the altitude. Standard values for different regions of Switzerland can be found in the SIA norm 384 [28]. Experimental measurements [47] show that the surface temperature in the lemanic region is $T_{g,s} = 11^\circ\text{C}$ (see Figure 47 in Appendix D).

Knowing the average depth of the geothermal wells, which is found to be $L_{gtw} = 267$ (see Section 4.1), the mean temperature in the geothermal well corresponds to $T_{g,mean} = 15^\circ\text{C}$.

It is assumed that the geothermal wells are well sized, in order to respect the natural recharge rate, which is strongly dependent on the type of soil. The sizing of the boreholes is very important to ensure a sustainable use of the ground heat throughout the years.

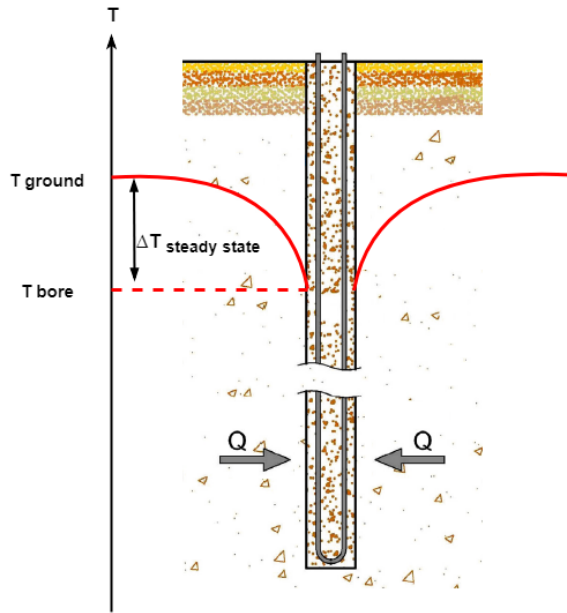


Figure 17: Steady state temperature difference in borehole, due to heat extraction

At any time heat is extracted from the ground, there is a temperature gradient that will form around the borehole, as shown in Figure 17. This temperature gradient depends on the heat extraction rate and the conductivity of the soil. Given the energy demand of the Eglantine district, it has been chosen to assume a negative temperature difference ($\Delta T_{steady state}$) of 3 °C [18, 27], due to the reduced cooling demand for this application. Thus the mean useful temperature of the

borehole over its depth is given by:

$$T_{b,mean} = T_{g,mean} - \Delta T_{SteadyState} = 12^\circ\text{C} \quad (50)$$

It has to be noted that this temperature gradient would be positive if the cooling demand is larger than the heating demand, thus resulting in an increase of the ground temperature.

The price for boreholes in Switzerland is found to be around $c_{wells} = 80$ [CHF/m] [48]. In order to provide the model with an energy dependent cost function, this value is transformed with help of the data from Table 32 in Appendix B:

$$L_{wells}^{tot} = n_{wells} * L_{well}^{average} \quad (51)$$

$$\text{Cost function [CHF/kW]} = c_{wells} \frac{L_{wells}^{tot}}{P_{hp}^{tot}} \quad (52)$$

where L_{wells}^{tot} is the length and n_{wells} the number of boreholes, and P_{hp}^{tot} is the total power of heat pumps installed.

The investment cost is calculated for summer use - the heat dissipated - as well as for the winter use - heat extracted, in function of the peak load of heating/cooling required. However, in reality the system is accounting twice for the same borehole, since the one for winter use will be the same during winter use. Thus, the total cost for the geothermal wells is chosen as the larger value between the two:

$$IC_{GTW} = \max (IC_{GTW}^{summer}, IC_{GTW}^{winter}) \quad (53)$$

The minimum approach temperature, necessary to exchange heat with the soil, can be determined with help of the procedure described in Section 3.4. The cost of the heat exchange area of the borehole is calculated assuming a standard pipe diameter of 32mm[28, 17]. The overall heat transfer coefficients of the well - including the fluid, the bore wall and the soil - are assumed to be [17]:

$$U^{g/water} = 9.3 \text{ kW/m}^2\text{K} \quad U^{g/CO2} = 17.1 \text{ kW/m}^2\text{K} \quad (54)$$

The resulting minimum approach temperatures are:

$$\Delta T_{min}^{g/water} = 14^\circ\text{C} \quad \Delta T_{min}^{g/CO2} = 6.8^\circ\text{C} \quad (55)$$

These values are similar to experimental or standard values found in literature [28, 49].

The water rise/drop in the water ground loop is assumed to be $dT_{water} = 4^\circ\text{C}$ [28]

4.3 External heat sources

The main advantage of a 5th generation district heating network is the ability to recover heat, and exchange it among the diversity of users. Two potential heat sources have been identified in the surroundings of the Eglantine district: the ice rink and a shopping mall. For the scope of this work, only the ice rink has been considered and studied.

4.3.1 Ice rink

An ice rink is a place where people can ice skate and play winter sports. The ice surface is normally inside an arena, which ensures comfortable temperatures for the people on the ice, as well as for the public, throughout the season. This also allows to extend the season, avoiding ice melt, when temperatures are warmer outside.

A study, conducted on more than one hundred ice rinks in Sweden, shows that the refrigeration system used to cool the ice surface has the largest share in total energy consumption, 43% (in average) as indicated in Figure 19 [51]. However, the ice rink often also includes changing rooms

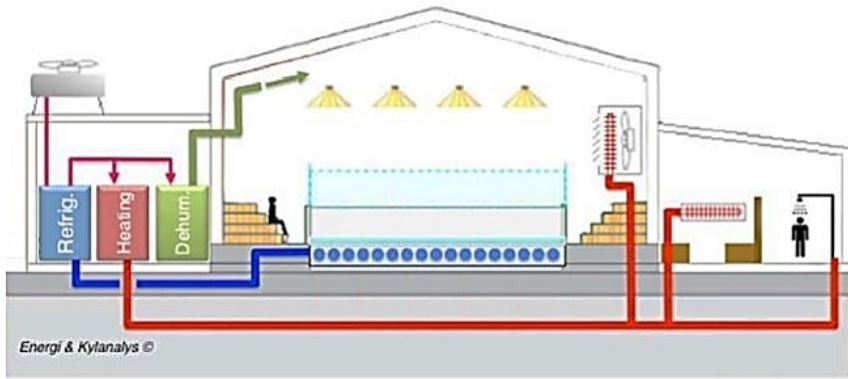


Figure 18: Energy system of a typical ice rink [50]

with showers, and a cafeteria or a restaurant, which also present heating demand. According to Figure 19, the average share of heating in the total energy demand is 26%. Last but not least, the ice surface has to be constantly illuminated, which requires a powerful lightning system. The global system is shown in Figure 18.

However, for practicality reasons, it is assumed that only the refrigeration system is connected to the CO₂ network, while the heating and electricity demand is supplied by the existing system, and are thus not considered in this model.

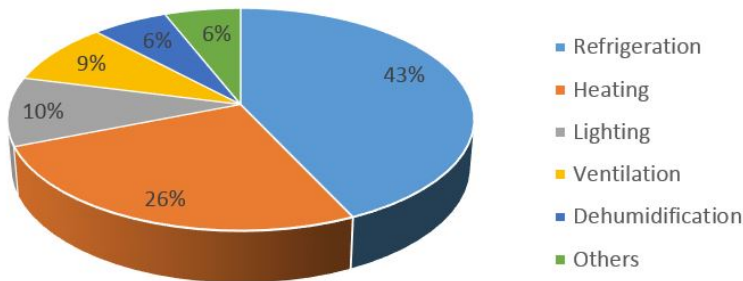


Figure 19: Energy demand of a typical ice rink [51]

Ice rinks are conventionally cooled with indirect systems, as shown in the right part of Figure 20, based on a ammonia (NH₃) vapor compression chiller, exchanging with a secondary brine loop that extracts the heat from the ice surface. The waste heat is normally, or at least in older systems, exchanged with the environment, with help of outdoor condensing units. Connecting it to a 5th generation district heating network, would allow recovering this heat and use it to cover the heat demand of other users. The connection to the CO₂ network is shown in the left part of Figure 20. This presents a high energy and exergy efficiency gain, since the refrigeration system can be driven on a lower and constant condensation temperature. However, assuming to recover heat from an existing cooling system, this gain is not considered in this work.

The calculation of the cooling demand of the ice rink is based on the following assumptions:

- Constant load profile throughout the ice season
- Ice season: 1st of August - 1st of April
- $COP_{ref} = 4$ [51]
- Ice surface = 1800m² [51]

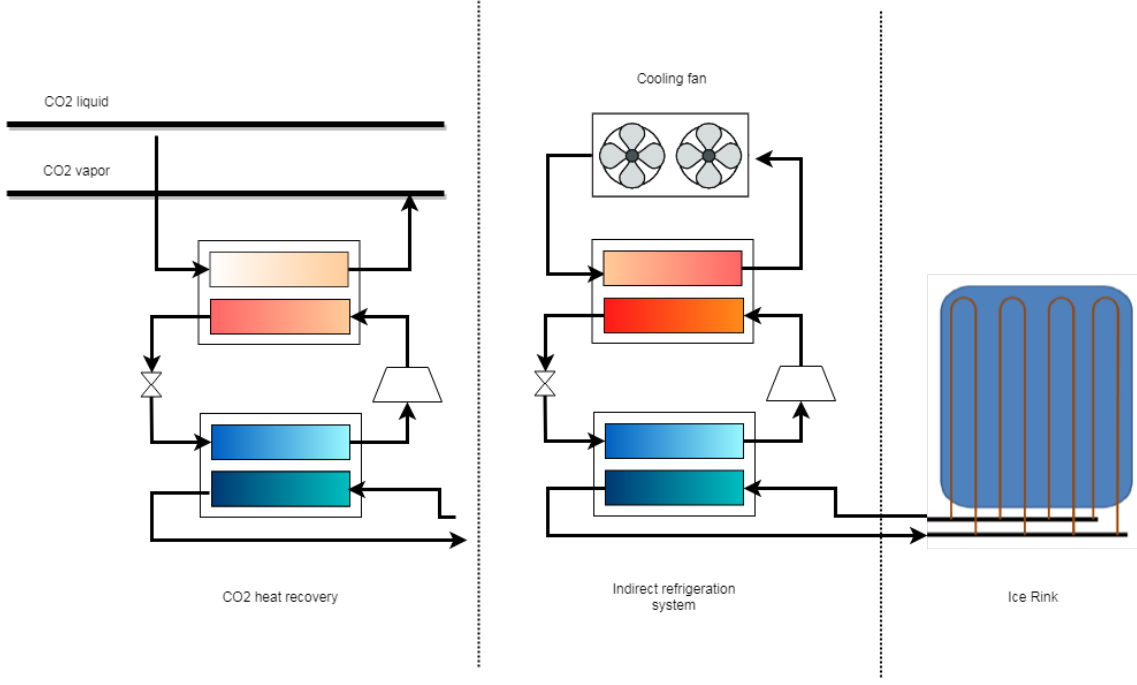


Figure 20: Refrigeration systems for ice rinks

- Specific cooling demand = $1\text{ kWh/m}^2/\text{day}$ [51]
- $dT_{min}(\text{refrigerant} - \text{ice}) = 1^\circ\text{C}$
- $dT_{min}(\text{refrigerant} - \text{refrigerant}) = 3^\circ\text{C}$

The daily cooling demand profile of the ice rink, is based on the required ice temperature, which varies throughout the day [51], as shown in Figure 21. Thus the computed ice cooling load profile is shown in Figure 22.

The total resulting waste heat rejected by the ice rink throughout the year corresponds to about 450 MWh/year .

Period	Rink function	T_{ice} [$^\circ\text{C}$]
0.00-6:00	Night setback	-1
6:00-8:00	Ice maintenance	-1
8:00-16:00	Low load	-3
16:00-18:00	Figure skating	-4
18:00-24:00	Hockey	-6

Figure 21: Ice rink refrigeration profile

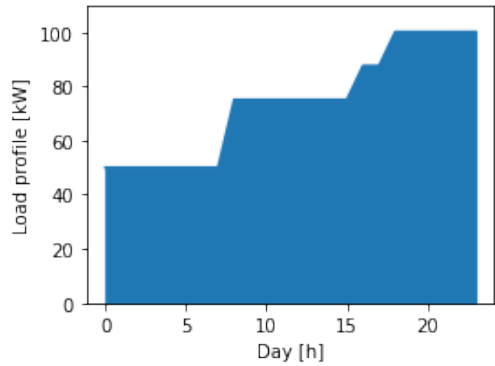


Figure 22: Ice cooling load profile of the ice rink, for a typical day

4.4 PV

The optimizer chooses the amount of PV that has to be installed (f_u^{PV}), according to the chosen objective function and parameters. This decision variable is sized to the total available roof area

(see Section 3.6.6). In some cases f_u^{PV} has been limited to 1, in order to let the optimizer use the total roof area, while in some other cases f_u^{PV} has been limited to 2, assuming that additional area (facades, parking lots, free area, etc.) would be available for the installation of PV panels. Table 8 shows the resulting PV area A_{PV} for those numerical examples.

Table 8: Numerical examples for PV area A_{PV} , in function of the available roof area A_{roof} and the decision variable of the optimizer f_u^{PV} (see Section 3.7).

f_u^{PV}	1	2
f_{area}	0.25	0.25
A_{roof}	11690 m ²	11690 m ²
A_{PV}	2923 m²	5845 m²

4.5 Energy conversion technologies

In order to evaluate the potential of alternative energy systems, three energy systems have been defined:

1. GS-HP: a set of decentralized geothermal heat pumps for heating, geo-cooling for space cooling and air-cooled compression chillers for refrigeration
2. GS-CO2DEN: CO2 based district energy network, with a central plant exchanging heat with the environment through a geothermal field
3. LS-CO2DEN: CO2 based district energy network, with a central plant exchanging heat with the environment through lake water

4.5.1 GS-HP

This energy conversion technology corresponds to a state of the art energy system for buildings and district, which is widespread in new buildings. Its schema is shown in Figure 23

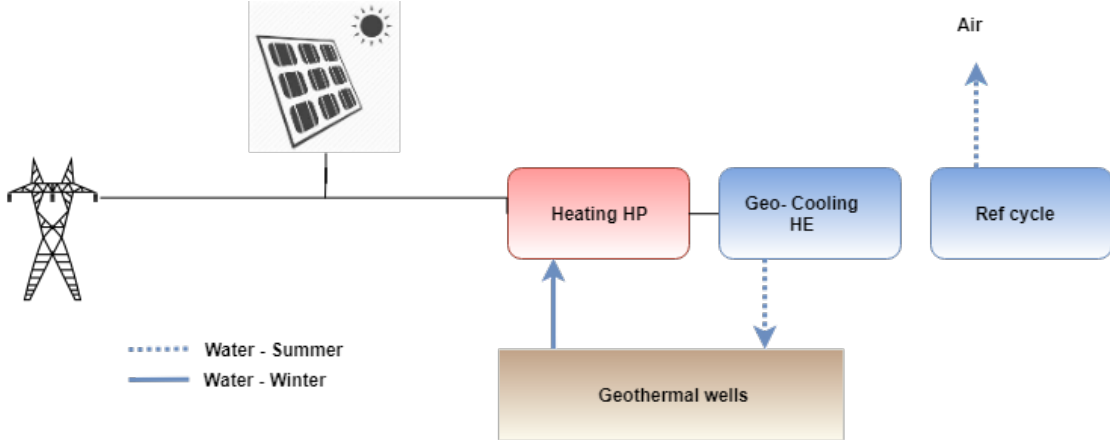


Figure 23: Schematic view of the GS-HP energy conversion system

The resource flows of the different units in the system are shown in Table 9.

The heating demand is supplied by a set of decentralized geothermal heat pumps, one for domestic hot water and one for space heating in every building. These heat pumps source the ambient heat from a secondary loop that exchanges heat with the ground through a system of geothermal wells, the SL-GSHP, which is described in Section 2.4.

Given the relevance of the heat pumps in the studied energy system, it has been chosen to use its thermodynamic model, which achieves more reliable and precise results.

Table 9: Resource flows for the reference energy system ((-): flow in / (+): flow out))

Units	Resource flows		
	Electricity	$Source_{hot}$	$Source_{cold}$
HP_{sh}	-	-	+
HP_{dhw}	-	-	+
HP_{ref}	-	+	-
HE_{ac}		+	-
Elec. Heater	-		
PV	+		
GTW_{winter}		+	-
GTW_{summer}		-	+

The temperatures at the evaporator and condenser are given by the following equations:

$$T_{evap} = T_{ground} - \Delta T_{min}^{ground/water} - \Delta T_{water} - \Delta T_{min}^{ref/water} \quad (56)$$

$$T_{cond} = T_{demand} + \Delta T_{min}^{ref/water} \quad (57)$$

where ΔT_{min} are the corresponding minimum approach temperatures, and ΔT_{water} is the temperature rise in the secondary water loop exchanging with the ground.

For the space heating heat pump, the refrigerant used is R123yf, as described in Section 3.6.2.

For the domestic hot water, it is chosen to use transcritical CO₂ heat pumps. As described in Section 3.6.3, this technology can achieve very good performances supplying heat that requires a high lift. This is the case in domestic hot water, where the water has to be heated from a temperature of 10 °C to a temperature of 55 °C.

Given the availability of geothermal wells, it has been chosen to implement geo-cooling for space cooling. The system is providing cooling at the ground temperature, corrected with the minimum approach temperature $\Delta T_{min,ground/water}$ and the temperature rise in the water loop ΔT_{water} .

$$T_{geo-cooling} = T_{ground} + \Delta T_{min}^{ground/water} + \Delta T_{water} \quad (58)$$

The refrigeration is achieved with a set of decentralized air cooled vapor compression chillers, which present the same working principle as heat pumps. The heat is evacuated into the environment with help of outdoor condensing units, as described in Section 3.6.4. The total energy consumption of the chillers is thus a sum of the energy demand of the compressor and the cooling fans:

$$\dot{E} = \dot{E}_{ref} + \dot{E}_{fans} \quad (59)$$

and the operating temperatures are defined in the following way:

$$T_{cond} = T_{amb} + \Delta T_{air} + \Delta T_{min}^{ref/air} \quad (60)$$

where T_{amb} is the ambient temperature, ΔT_{air} is the temperature difference of the cooling air between the input and the output of the condenser, while $\Delta T_{min}^{ref/air}$ is the minimum approach temperature difference needed for heat transfer between a refrigerant and air.

4.5.2 CO2DEN

The schema of the CO₂ network energy system is shown in Figure 24, while the main resource flows are shown in Table 10.

For space heating and domestic hot water, the same model as for the heat pumps in GS-HP are used. Since in this case the HP sources heat from the CO₂ network instead of the geothermal

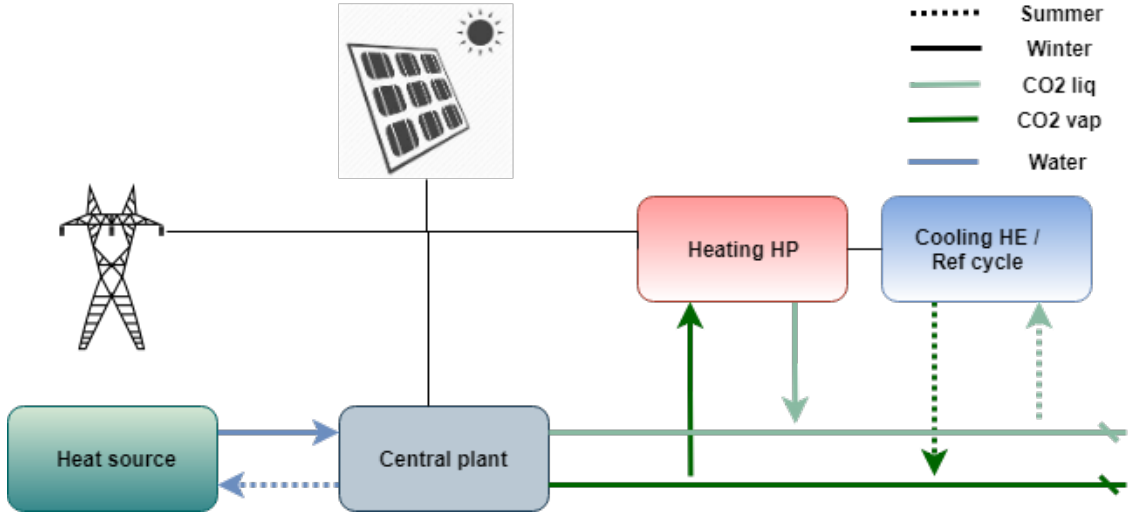


Figure 24: Schematic view of the CO2DEN energy conversion system

Table 10: Resource flows for the CO2 DEN ((-): flow in / (+): flow out))

Units	Electricity	Resource flows			
		$CO2_{liq}$	$CO2_{vap}$	$Source_{hot}$	$Source_{cold}$
HP_{cp}^{winter}	-	-	+	-	+
HP_{cp}^{summer}		+	-	+	-
HP_{sh}	-	+	-		
HP_{dhw}	-	+	-		
HP_{ref}	-	-	+		
HE_{ac}		-	+		
Elec. Heater	-				
PV	+				
GTW_{winter}				+	-
GTW_{summer}				-	+

wells, the major difference lies in the evaporation temperature, which corresponds to temperature in the CO2 vapor pipe ($T_{CO2,g}$):

$$T_{evap} = T_{CO2,g} - \Delta T_{min}^{ref/ref} \quad (61)$$

As for GS-HP, refrigeration is achieved through decentralized vapor compression chillers. However, in this case they are not air cooled, but they exchange directly with the CO2 network. Thus, the temperature in the condenser is given by:

$$T_{cond} = T_{CO2,l} + \Delta T_{min}^{ref/CO2} \quad (62)$$

Space cooling is provided by free-cooling, modeled by a simple heat exchanger that evaporates saturated liquid CO2, which is then injected back into the network in a superheated vapor state. The mass flow of the CO2 is adapted to satisfy the cooling demand. It is assumed that pressure and temperature losses are negligible.

As mentioned before, heating and cooling loads in the system are not always balanced. Thus, there is the need for a central plant (CP) to balance out the system, able to heat and cool. A centralized heat pump is very suitable for this purpose. This HP has been modeled with its thermodynamic model (see Section 3.6.2). In order to have a HP model for the central plant that is able to handle different source temperatures, different operating modes have been implemented.

Otherwise, computation problems arise when the source temperatures reaches the condensation temperature of the heating part of the CP, which corresponds to the temperature of the CO₂ network. In the same way, this higher source temperature also precludes the possibility of free-cooling. However, if the temperatures is higher than the CO₂ network, the central pump might be able to source heat without operating a heat pump (free-heating). The model includes two operating modes - heat pump HP or heat exchanger HE - for each part of the central plant, the heating part (CP-winter) and the cooling part (CP-summer). The parameters that vary in function of the operating modes are the electricity consumed E_{cp} and the investment cost parameters.

The thresholds temperatures are set in the following way:

$$T_{thresh}^{free-cooling} = T_{CO2} - \Delta T \quad (63)$$

$$T_{thresh}^{free-heating} = T_{CO2} + \Delta T \quad (64)$$

where ΔT is the minimum temperature difference needed for the specific heat exchange.

The operating modes are shown in Table 11.

Table 11: Operating modes to determine if the CP operates in heat pump (HP) or in heat exchanger (HE) mode, depending on the borehole temperature and the threshold temperatures for free-cooling T^{FC} and free-heating T^{FH}

$T_{borehole}$	$\leq T^{FC}$	$T^{FC} \leq T \leq T^{FH}$	$\geq T^{FH}$
CP-winter	HP	HP	HE
CP-summer	HE	HP	HP

Two different heat sources have been considered for this energy conversion technology: the lake and a geothermal field. For the geothermal CP a direct expansion system is assumed (see Section 2.4), while for the lake water CP a R1234yf HP is used. A schematic representation of the CO₂ DEN with DX-GSHP technology is shown in Figure 46, in the Appendix C.

4.6 Numerical application

4.6.1 Cost functions

As described in Section 3.7, the model need investment cost parameters that can be calculated with the procedure explained in Section 3.3. Values for the heat pumps are given in Henchoz et al., obtained by linearizing commercial products [43]. The cost function for heat exchangers has been interpolated in order to have a function dependent on the amount of exchanged heat.

Values are summarized in Table 12.

Table 12: Summary of the investment cost function of each technology, including their expected lifetime and the interest rate.

Technology	Cost function [Euro]	X [unit]	Interest rate	Lifetime
HP	1'240 X + 5680	E_{comp} [kW]	0.08	20
Heat exchanger	215 X + 56	Q [kW]	0.08	20
Electric heater	23 X + 968	Q [kW]	0.08	20
PV	300 X	A [m^2]	0.08	20
Geothermal wells	2890 X + 5800	Q [kW]	0.03	50
Network	See Section 3.6.7			

Operating costs are calculated through the exchange with the electricity grid, using the cost of electricity shown in Table 13. It has also to be noted that for the scope of this work it has been assumed that the fixed part of the operating costs c^{op2} (see Section 3.7) is negligible.

Table 13: Buying and selling cost of electricity [52].

Electricity price	c_{el} [Euro/kWh]
Buying	0.2
Selling	0.1

4.6.2 Minimum approach temperature

As seen in Table 3, CO2 (R744) has a higher heat transfer coefficient than other conventional refrigerants, as for example R1234yf. This has to be taken into account in the energy system through a different minimum approach temperature. To do so, there are two possible approaches:

- calculate a new, lower, ΔT_{min}^{R744} , maintaining the same heat exchange area A_{ex} . This results in higher COP for the heat pump and thus lower operating costs OC_{hp}
- calculate a new, smaller, heat exchange area A_{ex} , maintaining the same ΔT_{min} . This leads to lower upfront costs IC_{ex}

It is chosen to use different ΔT_{min}^{R744} , maintaining the same heat exchange area, in order to show the difference in terms of performance gain, rather than in financial gain. The following procedure is repeated for the various fluids (X) the refrigerants have to exchange with:

1. Calculate $U_{R1234yf/X}$ with Equation 8
2. Optimize $\Delta T_{min}^{R1234yf/X}$ with numerical values from the Eglantine district, as described in Section 3.4
3. Calculate $U_{R744/X}$
4. Solve Equation 5 in function of ΔT , using $U_{R744/X}$ and the A_{ex} resulting from the previous step.

The implementation of this algorithm has been solved on *Matlab* with help of function *solve(equation 5, ΔT_{min})*. Thus resulting ΔT_{min} values shown in Table 14.

Table 14: Minimum approach temperatures used for heat exchanges in the model

ΔT_{min} [K]	Ground	Water	R744	R1234yf
Water	14	-	-	-
R744	6.8	3.46	0.8	-
R1234yf	-	4	1.4	2.3

As example, Figure 25 and Figure 26 show the resulting optimization of the minimum approach temperatures, respectively for refrigerant and ground heat exchanges. The straight vertical line shows the optimum ΔT_{min} for the reference heat exchange, in function of the total costs (green line), while the dashed line shows the improved ΔT_{min} for CO2, maintaining the same A_{ex} .

As expected, the resulting minimum temperatures for heat exchanges with CO2 are lower, implying a decrease in the exergy losses in heat exchanges. This is very important to account for the gain in performance given by the use of the CO2 network, with respect to the refrigerants used in the concurrent energy conversion technologies.

4.6.3 Compressor efficiencies

The compressor efficiencies are directly calculated in the model, according to the equations in Section 3.6.3 and 3.6.2 in function of P_d and P_s , respectively the pressure of discharge and suction of the compressor. Table 15 shows the resulting efficiencies for the average day in January, for the different heat pumps used in this work.

These values are similar to reference values found by Yang et al.[40] in their experimental work.

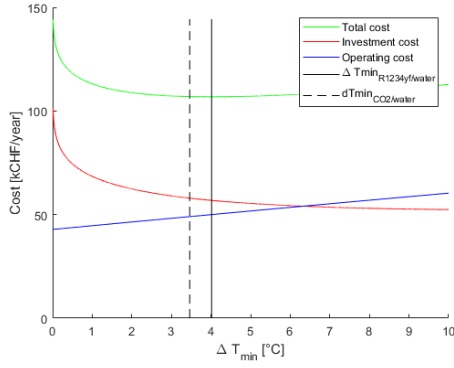


Figure 25: Optimization of ΔT_{min} values for heat exchange with refrigerant R1234yf, through minimization of total costs (green line)

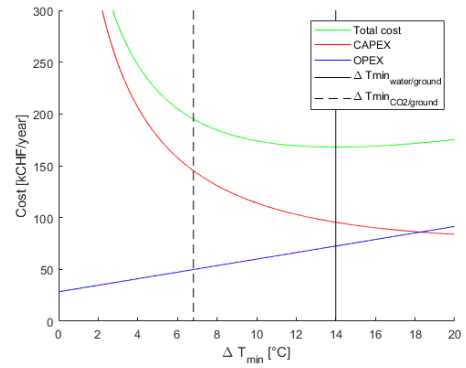


Figure 26: Optimization of ΔT_{min} values for heat exchange with the ground, through minimization of total costs (green line)

Table 15: Calculated efficiencies for heat pump compressors, during an average day in January

Unit Refrigerant	CO2 DEN					Reference scenario		
	CP R123yf	CP CO2	SH R123yf	DHW R744	REF R123yf	SH R123yf	DHW R744	REF R123yf
P_d	5.0	43.0	9.4	84.9	5.0	9.4	66.0	11
P_s	2.4	20.2	4.6	46.7	2.80	2.4	30.4	2.4
η_{mech}	0.85	0.80	0.85	0.78	0.85	0.85	0.80	0.85
η_{is}	0.85	0.70	0.85	0.71	0.85	0.82	0.70	0.81
η_{comp}	0.72	0.56	0.72	0.55	0.72	0.70	0.56	0.69

4.6.4 Direct expansion HP

As discussed in Section 2.4, there is the possibility to directly expand the CO₂ into the geothermal well, instead of exchanging with help of a secondary water loop. To grasp the increase in performance, a simulation is performed on the CP of the CO₂DEN technology. The used parameters, refrigerants and temperatures are shown in Table 16. The CO₂ heat pump has lower compressor efficiencies (see Table 15), which results in a lower η_{COP} . However it has a much lower temperature difference to cover, thanks to the direct expansion of the CO₂, achieving a much higher COP value.

Table 16: Comparison of simulation results for a SL-GSHP, versus a DX-GSHP

-	SL-GSHP	DX-GSHP
	R1234yf	R744
T_{source}^{lm}	12	12
T_{demand}^{lm}	35	35
T_{cond}^{lm}	16.4	15.8
T_{evap}^{lm}	-9.4	5.2
COP_{real}	6.5	15.8
η_{COP}	65 %	60 %

4.6.5 Recalculation of the COP efficiency

Running the optimization using heat pump models based on the thermodynamic cycle (see Section 3.6.2) provides a very accurate results, but requires more time consuming calculations. De-

pending on the application - for example for rough estimations at the beginning - it can be interesting to use the simplified model based on the carnot cycle instead (see Section 3.6.1). Thus, it is found useful to recalculate the COP efficiency η_{COP} values for all the concerned heat pumps, with respect to the operating conditions needed in this work. The calculation is straightforward, with the following equation:

$$\eta_{COP} = \frac{COP_{real}}{COP_{theoretical}} \quad (65)$$

Table 17: Recalculated η_{COP} values, with its operating temperatures

Unit	CO2 DEN					Reference scenario		
	CP	CP	SH	DHW	REF	SH	DHW	REF
Refrigerant	R123yf	CO2	R123yf	R744	R123yf	R123yf	R744	R123yf
T_h	16.5	15.8	39	37.1	16.5	39.8	41	28.7
T_c	-9.4	5.2	11.5	11.5	2	-5	5	2
η_{COP}	0.65	0.6	0.693	0.512	0.624	0.688	0.708	0.56

The new values are shown in Figure 17.

5 Results and discussion

5.1 Energy and exergy performance

A direct way to compare the performance of the different conversion technologies is the coefficient of performance, which is simply given by the ratio between the delivered heat Q and the consumed electricity E . The *heating*, *cooling* and *global* COP values are calculated in the following way:

$$COP_{heating} = \frac{Q_{SH} + Q_{DHW}}{E_{SH} + E_{DHW} + E_{CP,winter}} \quad (66)$$

$$COP_{cooling} = \frac{Q_{REF} + Q_{AC}}{E_{REF} + E_{CP,summer}} \quad (67)$$

$$COP_{global} = \frac{Q_{SH} + Q_{DHW} + Q_{REF} + Q_{AC}}{E_{SH} + E_{DHW} + E_{REF} + E_{CP,tot}} \quad (68)$$

where $E_{CP} = 0$ for the GS-HP.

The values, calculated in each time step, are shown in Figure 27. If the temperatures of evaporation and condensation of a heat pump are fixed, the operating cycle is also fixed, and thus the COP value. However, the temperature of the heat demand rises with the amount of heat required and a fixed condensation temperature would imply high exergy losses, given that most of the time the approach temperature would be larger than the minimum required one. Modern HP can therefore adapt their operating cycle in order to fit the varying heat demand temperature. This results in non-constant COP value, as it can be seen for the SH HP (blue line), which varies between 6 and 14. The same happens to the compression chillers in the GS-HP, which perform worse during summer, when they have to deliver heat to a higher ambient temperature. In comparison, the COP of refrigeration in the CO2DEN are constant, since heat is delivered at a constant temperature throughout the year to the CO2 network.

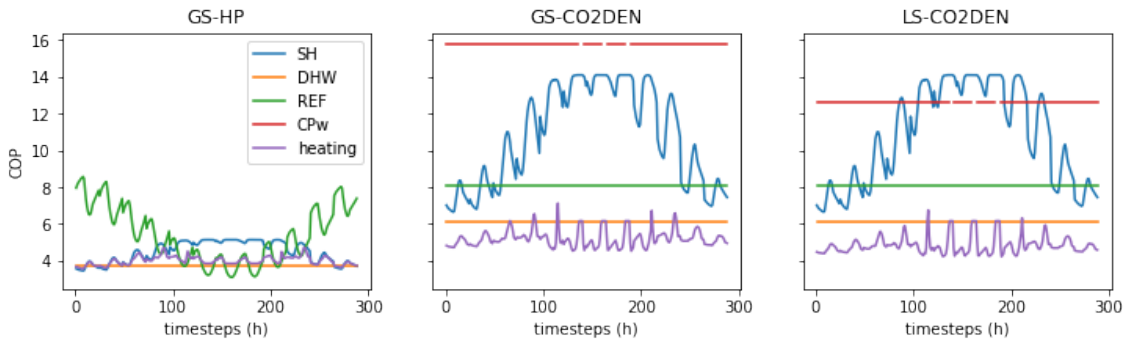


Figure 27: Comparison of COP values for each time step t and unit. The *cooling* and the *global* COP are not displayed given the different order of magnitude due to the free cooling

The COP for the heating heat pumps SH and DHW are considerably higher in the CO2DEN. This is due to the "two stages" of the conversion technology: the heat is first furnished to the CO2 network by the CP and then brought up to the required temperature by the decentralized HP. Thus to consider the resulting COP for heating facilities, the values from the CP, SH and DHW would have to be combined. The COP of the central plant is higher in the GS CO2DEN, being the evaporation temperature higher than in the heat exchange with the lake.

The mean COP values for each technology are shown in Table 18. The GS-CO2DEN shows the best performance with a global COP of 6.1. The LS-CO2DEN follows with 5.6 and the GS-HP with 4.6. The increase in the global COP is reflected in a reduced electricity consumption by the energy system; this is shown in Table 19. With respect to the GS-HP, the GS-CO2DEN requires 24% and the LS-CO2DEN 17% less electricity.

Table 18: COP values for the three energy system

	GS-HP	GS-CO2DEN	LS-CO2DEN
HP-SH	4.5	10.8	10.8
HP-DHW	3.8	6.2	6.2
HP-REF	5.4	8.1	8.1
HP- CP_{winter}	-	15.8	12.6
Heating	4.0	5.2	4.9
Cooling	19.1	50.4	50.4
Global	4.6	6.1	5.6

Table 19: Electricity consumption of the three energy conversion technologies

	GS-HP	GS-CO2DEN	LS-CO2DEN
Electricity consumption [kWh/yr]	611'000	472'000	510'000
Corresponding reduction	-	23%	17%

The exergy values of supply and demand have been calculated for each conversion technology, as explained in Section 3.5. This analysis shows the real thermodynamic value of the required energy services, since not only the amount of heat is considered, but also the temperature level at which it happens. The exergy value of the demand is thus calculated in function of the varying ambient temperature and is the same for all technologies.

The exergy efficiency for the different energy conversion technologies are shown in Table 20. It is clear to see that the GS-HP performs worse than the CO2 technologies with 24%, against 32% of the GS-CO2DEN and 30% of the LS-CO2DEN. This difference is explained by the lower exergy efficiency of the GS-HP, which presents higher minimum approach temperatures, as well as a lower COP of the heat pumps. The reason for the high performance of the GS-CO2DEN, despite having two stages and thus some additional losses due to ΔT_{min} values, is the direct expansion of CO2. As shown in Section 4.6.4, the energy and exergy gain, with respect to the conventional system based on a secondary water loop, are indeed remarkable.

Table 20: Comparison of the exergy losses \dot{L} and efficiencies η_{exergy} for the different energy conversion technologies

-	units	GS-HP	GS-CO2DEN	LS-CO2DEN
\dot{L}_{tot}	[MWh]	1500	1003	1136
η_{exergy}	[%]	24%	32%	30%

Figure 28 shows the exergy efficiency for the different conversion technologies, calculated for each time-step - the values are sorted in decreasing order. It can be seen that the exergy efficiency is dependent from the operating temperatures, as well as from the ambient temperature. Thus the exergy efficiencies vary between 10-50% throughout the year. Moreover, the graph shows that the quality of the energy system, i.e. the order of best and worst performing technologies, remains the same during all time steps.

5.2 Financial analysis

A financial analysis of the three conversion technologies is shown in Figure 29. The used cost functions, energy prices and maximal available PV area are given in Table 21.

Given that in this work the cost of operation (OC) depends only from the consumed electricity (no consumption of gas or other resources), this is directly correlated to the global COP of the system. As seen above (see Table 18), GS-CO2DEN presents the highest coefficient of performance

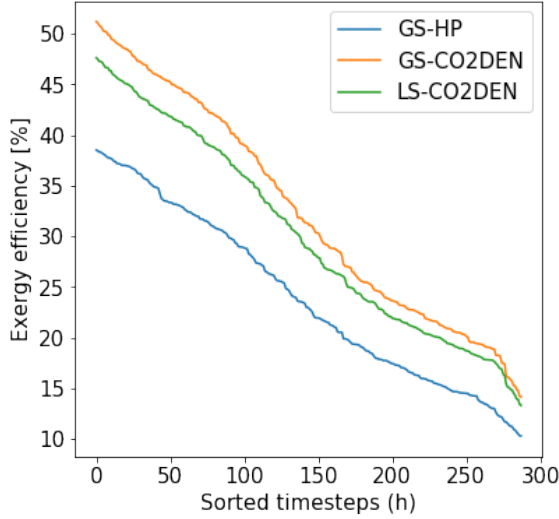


Figure 28: Exergy efficiencies calculated in each time step - sorted in decreasing order

Table 21: Summary of relevant cost and decision constraints.

Cost functions	Table 12 in Section 4.6.1
Electricity cost	Table 13 in Section 4.6.1
Max. PV area available	2923 m^2 (see Table 8 in Section 4.4)

and thus also the lowest OC (dashed line), with 260'000[*Euro/yr*], and GS-HP the highest with 290'000[*Euro/yr*]. The LS-CO2DEN presents an OC of 270'000[*Euro/yr*].

The investment costs are shown more in detail in the clustered columns. It is easy to note that the GS-HP has much lower upfront costs (180'000[*Euro/yr*]) than the GS-CO2DEN solution (220'000[*Euro/yr*]). Indeed, due to the higher COP values, a larger share of heat comes from the geothermal wells, which increases their investment cost. Moreover, there is the additional cost of the CO2 pipes needed to connect all the user. In the SL-CO2DEN there are obviously no costs related to the geothermal wells, but the cost for the water pipes that allow the water to be brought to the CP. Given the actual distance of the Eglantine district from the lake, this solution leads to much higher upfront costs than the competing technologies (310'000[*Euro/yr*]).

Despite the lower OC for the CO2DEN technologies, the total cost is clearly following the tendency of the IC, which present a larger difference. The GS-HP ends up being the cheapest variant with 470'000[*Euro/yr*], followed by the GS-CO2DEN with an only slightly higher cost of 485'000[*Euro/yr*]. The SL-CO2DEN is the most expensive solution with 580'000[*Euro/yr*].

Self consumption and autarchy do not vary much between the technologies, because no storage technology has been taken into account. Indeed, any kind of storage - thermal, electrical or CO2 - would enable to adapt the consumption to profit from the cheap domestic produced energy, as well as to reduce peak demands. Moreover, despite of the optimizer choosing install the maximum possible amount of PV - which corresponds to the roof surface - for the three technologies, in order to reduce the OC, the amount of electricity produced is seldom larger than the total electricity demand of the district. Thus, the three systems have an autarchy of about 25%, and a self consumption rate of around 95%.

For what has been seen in this section, the CO2 network showed an excellent energy performance. However, the reasons to opt for such a technology will have to go beyond financial arguments, since it remains a more expensive solution, even if this could quickly change if the

price of electricity rises, which is not such a far-fetched scenario. Another strong argument in favor of this technology is the space planning. A city center might first of all not have the space for, but also not want everyone to drill boreholes under its house. The CO₂ network would allow to profit from its benefits, while outsourcing and give flexibility to the planning and realization of the geothermal field.

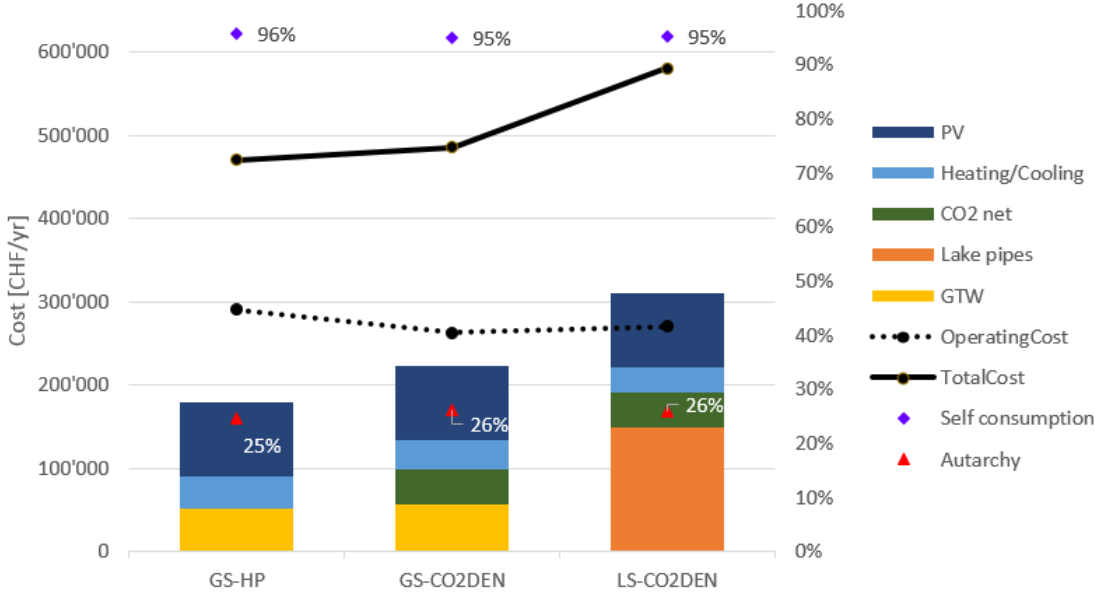


Figure 29: Cost comparison for the three different energy systems variants

5.2.1 Parametric optimization of GS-HP

A parametric optimization of the costs of the reference energy system (GS-HP) is shown in Figure 30. The optimizer is let to optimize the operating costs, while step-wise constraining the investment cost. This is a help for decision making. The used cost functions, energy prices and maximal available PV area are given in Table 21.

Table 22: Summary of relevant cost and decision constraints.

Cost functions	Table 12 in Section 4.6.1
Electricity cost	Table 13 in Section 4.6.1
Max. PV area available	5845 m ² (see Table 8 in Section 4.4)

It can be seen that the biggest difference in investment and operating cost is due to the sizing of the PV - for which an increased area is considered in this case (see Table 22), accounting for potential facades and free space PV. When constraining the investment costs, the model installs only a small share of PV, which increases the operational costs. On the contrary, a high share of PV increases the systems rate of auto-sufficiency, lowering the operational costs.

On the far right, the maximum allowed share of photovoltaic (PV) is reached. However, the operational are additionally lowered thanks to a different handling of peak consumption. The optimal system installs a small share of electrical heater (R-EL) to cover peak demand, which allows to optimally size the heating heat pumps (HP-SH, HP-DHW). In the last column on the right, the system chose not to install the electrical heater but installing larger heat pumps, which strongly increases upfront costs, but allows to further reduce the operational costs.

On the far left, the opposite phenomenon happens, i.e. no PV are installed to reduce the investment costs. To further reduce upfront costs, the system chose to cover the heat demand almost entirely with help of the electric heater, minimizing the size of the heating heat pumps.

The optimum, with respect to the total cost of the energy system, is in the very middle of the graph, between column 2 and 3. The optimum is analyzed in the following chapters.

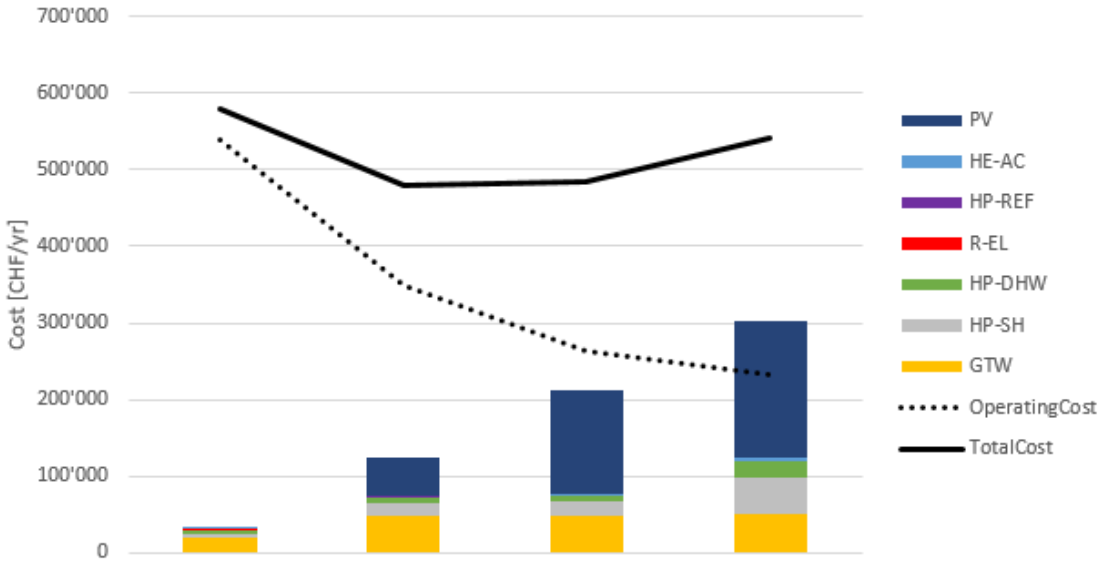


Figure 30: Parametric optimization of the reference energy system (GS-HP), showing the detailed investment costs, the operational cost and the total cost.

5.2.2 Parametric optimization of GS-CO2DEN

A parametric optimization of the costs of the CO₂ district energy system with ground sourced central plant (GS-CO2DEN) is shown in Figure 31. The optimizer is let to optimize the operating costs, while step-wise constraining the investment cost. This is a help for decision making. The used cost functions, energy prices and maximal available PV area are given in Table 21.

The response of this system to the parametric optimization is very similar to the one of the GS-HP system. This means that the biggest difference in investment and operating cost is due to the sizing of the PV - for which an increased area is considered also in this case (see Table 22) -, while the extreme cases are determined by the ratio between the electrical heater and the heating heat pumps. The optimum is analyzed in the following chapters.

In order to discuss the validity of the results, the investment costs have been benchmarked against two other existing anergy networks in Switzerland - the *Anergienetz ETH Hönggerberg* and the *Anergienetz Friesenberg*. This is done by comparing the share of the total cost represented by the network, the geothermal wells and the heating and cooling facilities. The resulting percentages are shown in Table 23. It can be seen that the GS-CO2DEN system in the Eglantine district presents a much lower percentage of the investment cost $IC_{Heating/cooling}$ attributed to the heating and cooling equipment (HP-SH, HP-DHW, HP-REF, HE-AC), with respect to the other two networks. This leads to higher shares of investment costs attributed to the CO₂ network and the geothermal field.

One reason for this difference is most likely the size difference between the energy systems. In fact, the Eglantine system is drastically smaller than the one at ETH or in Friesenberg, which have a heating demand which is respectively 12 and 15 times bigger. The specific investment costs for building the network and drilling the geothermal wells decreases with size - for example the costs of digging to place a pipe underground won't be strongly correlated with the pipe diameter. On the contrary, the specific costs for the heat pumps will stay about the same, given that the size of the decentralized heat pumps will not increase, only its number.

On the other hand, it is not trivial to estimate the cost of building the CO₂ network, given the lack of real applications, and the resulting costs could be proven to be inaccurate. Also the sizing

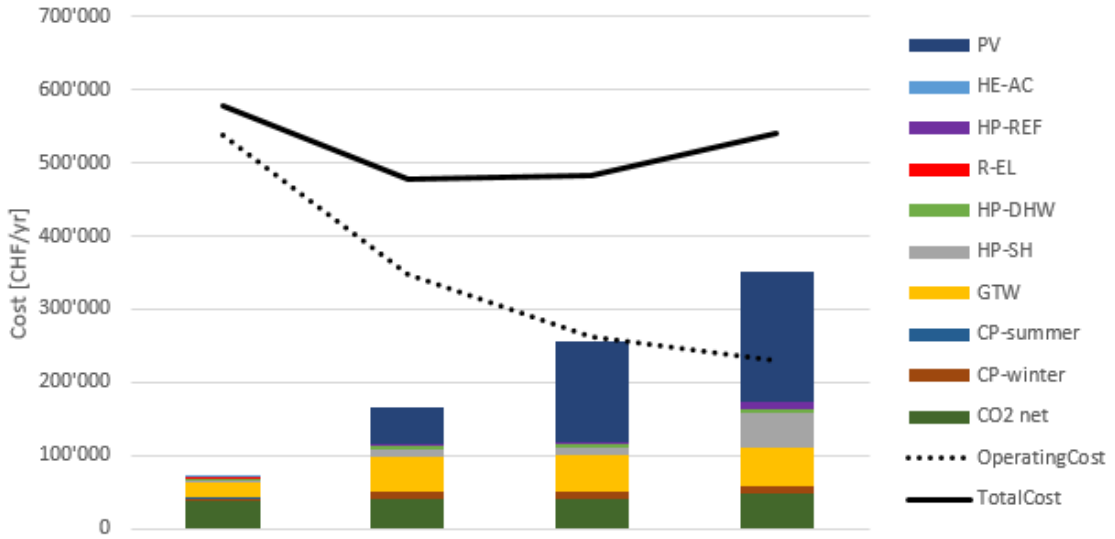


Figure 31: Parametric optimization of the ground sourced CO2 DEN (GS-CO2DEN), showing the detailed investment costs, the operational cost and the total cost

Table 23: Cost comparison with existing anergy systems

	Eglantine	Anergienetz ETH Hönggerberg	Anergienetz Friesenberg	
IC_{NET}	[%]	31.4 %	18.1 %	25.9 %
IC_{GTW}	[%]	42.1 %	32.7 %	23.5 %
$IC_{Heating/Cooling}$	[%]	26.5 %	49.2 %	50.6 %
Heating power	[kW]	592	8'000	3'930
Heating demand	[MWh/yr]	2'390	28'450	35'000
Cooling power	[kW]	84	6'000	3'500
Cooling demand	[MWh/yr]	33	26'200	80'000

of the geothermal well, in order to account for yearly energy balance and recharge rate, and for the specific cost, according to depth and soil type would have to be verified and confirmed through further studies and simulations.

5.3 Heat source integration

The integration of large external heat sources, as for example an ice rink, is very interesting for a CO2 district energy network, since heat recovery allows to reduce the load of the CP, and thus the load of the heat source. It has been assumed that the existing facility already exists, and therefore its energy demands are not included in the model. This means that also the gain in performance of the cooling system, through the lower condensation temperature obtained by exchanging with the CO2 network, is not taken into account. The external heat source is purely considered as a free heat source. The used cost functions, energy prices and maximal available PV area are given in Table 21.

Figure 32 shows the heat demand of the system (upper row) and the heat exchange with the heat source (lower row), by comparing the system before (left column) and after (right column) the integration of the ice rink. The additional cooling demand of the ice rink is shown in red. The increased cooling demand reduces the amount of heat that has to be furnished by the CP, thus reducing the total energy demand of the system - the global COP raises from 6.12 to 6.73. This also means that less heat will be extracted from the geothermal wells: this is reflected in the reduction of the orange area in the lower row, which corresponds to the amount of heat that is

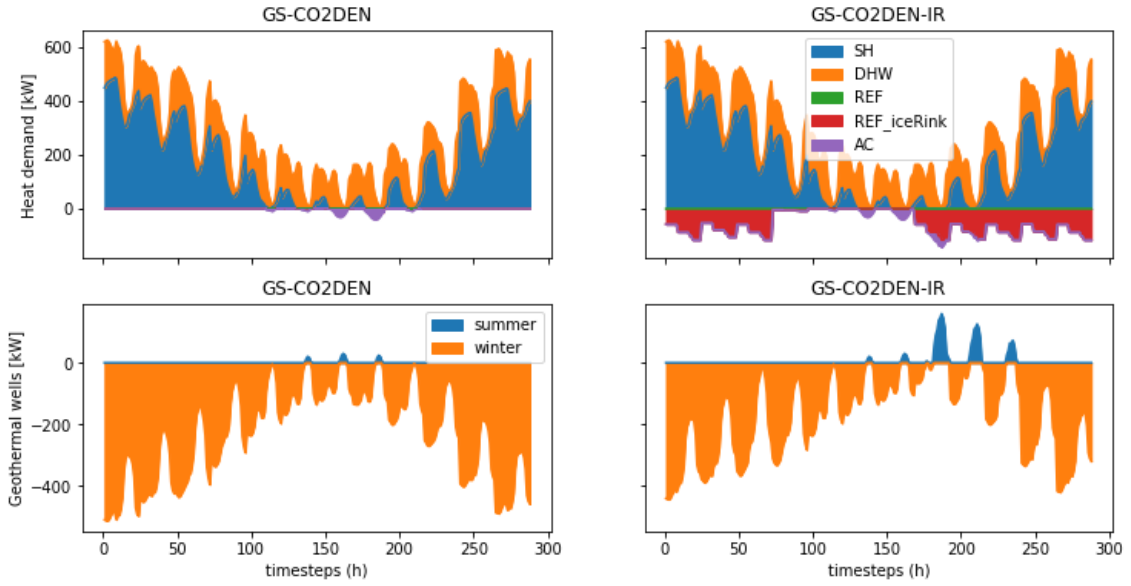


Figure 32: Comparison of the heating (+) / cooling (-) demand - upper row - and the heat extracted (+) / injected (-) into the boreholes - lower row - before - left column - and after - right column - integration of the ice rink

extracted from the source, throughout the year.

An analysis of the economic differences caused by the integration of the ice rink is shown in Figure 33. The reduced use of the CP lowers the electricity demand of the heating/cooling facility from 470'000 to 435'000[kWh/yr] - which corresponds to a reduction of 9%. At the same time, the lower peak use of the GTW reduces its IC. On the other hand, the integration of the external heat source requires the installation of additional CO₂ pipes, which has an impact on the upfront costs. The resulting difference in the total cost is negative, i.e. the total cost of the CO₂ energy network is lower if the ice rink is connected, by about 4'000 [Euro/yr]. This is not yet sufficient to have a lower cost than the GS-HP, but its reducing the gap to about 10'000 [Euro/yr]. Note that, as mentioned before, the reduction in operating costs in the ice rink cooling facility has not been taken into account.

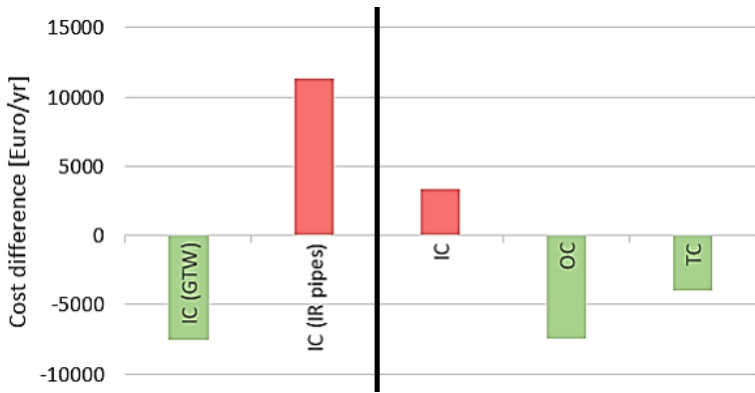


Figure 33: Cost difference of the GS-CO2DEN with and without ice rink. Positive values (+) reflect a higher, and negative values (-) a lower cost originated by the IR integration.

Figure 34 shows the shares of electricity consumption, on a sorted time axis. What is interesting to note is the shares of electricity consumption between the CP and the decentralized HP. E_{cp} represents around 10% of the global electricity consumption, and around 30% of the $E_{heat/cool}$.

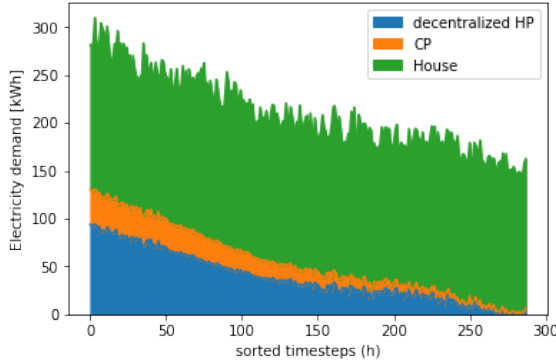


Figure 34: Electricity demand of GS-CO2DEN system grouped in categories, sorted in decreasing order

This means that even a system having a perfectly balanced heating and cooling demand would not be able to reduce its OC of more than 30%, since, as far as the temperature of the CO₂ network remains constant, the operating conditions of the decentralized heat pumps remain unchanged too.

Furthermore, it is important to account for uncertainties bound to the external heat source. For example for an ice rink, the replacement of the obsolete and inefficient cooling facility, or an improvement in the facility management, can drastically reduce its energy. Same for other potential heat sources as industrial processes, which can be improved or replaced over time. This should be considered in the inclusion of external heat source, since a reduction, or the absence, of the additional heat could threaten the functioning of the system.

5.4 Ground temperature response

A critical parameter for the efficiency of a ground sourced energy system is the ground temperature. As seen in Section 3.2, this temperature depends mainly on the depth, the temperature gradient in the given soil and the surface temperature. In other words, it is dependent from the location - including local climate and altitude - and the depth of drilling. In order to acknowledge the influence this temperature has on the system's performance, a sensitivity analysis has been performed. The results are shown in Figure 35. The used cost functions, energy prices and maximal available PV area are given in Table 21.

The GS-HP energy system seems to respond in a linear way to the temperature raise, as it can be expected, thanks to the lower required temperature raise for heating, which increases the COP of the system. In reality a small step can be identified between 14 and 15 °C,

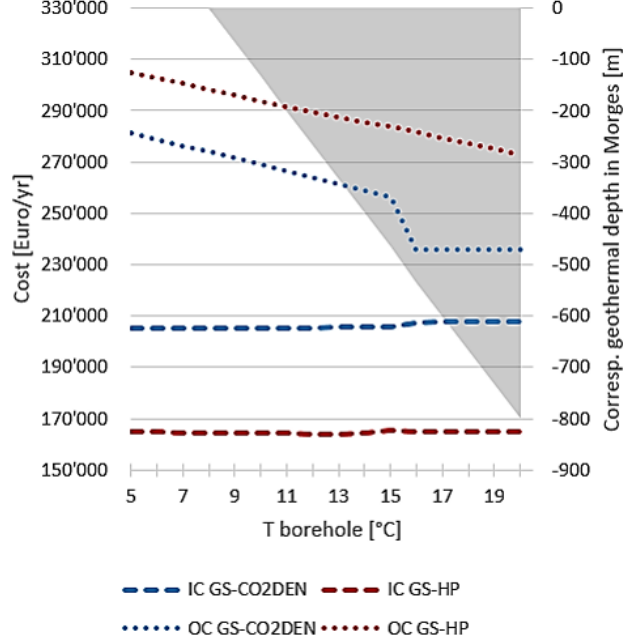


Figure 35: Cost comparison of variants in function of the borehole temperature. The gray area represents the geothermal depth - in the Lemanic region - that corresponds to a given temperature

at which the IC drop and the OC rise. This step happens when the ground is not cool enough anymore to offer the option of free-cooling. The system is forced to use a refrigeration system instead, which increases the OC. However this utility is already installed, and thus the increase of IC_{HP-REF} is lower than the reduction of the obsolete IC_{HE-AC} .

The GS-CO2DEN energy system presents a more evident step in its response to the ground temperature. The reason lies in the use of the central plant, which, as described in Section 4.5.2, has different operating modes for cooling and heating. In fact, if the temperatures are either high or low enough, it can operate free-cooling or free-heating. In any other case, it operates in cooling and/or heating HP mode. In this case the step happens at $T_b \geq 16^\circ\text{C}$, for which the CP can source heat directly from the ground without the need of a heat pump, which drastically reduces the operational costs.

Assuming uniform soil and maintaining a constant heat capacity, a higher borehole temperature would imply drilling a smaller number of wells with greater depth. In other words, the geothermal model described in Section 3.2 simply models the heat capacity and the investment cost per borehole meter. It is thus not able to properly account for advanced correlations between heat capacity, cost function and well depth. Moreover the regeneration rate of the soil should be considered, in order to properly model its temperature, in function of the heat extracted throughout days, seasons and years.

Nevertheless, this sensitivity analysis gives an idea of the global behavior response of the different conversion technologies to the ground temperature. This can be very helpful to estimate the performance of either system, in function of the geographical location, latitude and altitude.

5.5 Lake distance

As it has been seen in the Section 5.1, the LS-CO2DEN presents competitive OC. However its investment costs strongly depend on the necessary pipe length. Therefore, there will be a distance under which the LS-CO2DEN presents a lower total cost than the concurrent systems. This threshold distance depends on the ground temperature, given that the TC of the GS-HP and the GS-CO2DEN vary accordingly. The resulting thresholds are plotted on Figure 36. This helps choosing between using the lake or the soil as a heat source, knowing the mean ground temperature and the distance from the lake water.

At $T_{borehole} = 12^\circ\text{C}$, as in the Eglantine district, the LS-CO2DEN would be a financially interesting solution against GS-HP and GS-CO2DEN if the distance to the lake is respectively shorter than 328 and 484 meters.

The used cost functions, energy prices and maximal available PV area are given in Table 21.

5.6 Optimization of energy demand

The Eglantine district is composed for 97% of buildings dedicated to residential use (see Section 4.1), resulting in a very low cooling and refrigeration demand. It is now legitimate to wonder how the different energy systems would perform in a different district, i.e. with a different building use and thus a differently composed energy demand. In this chapter, it will be tried to answer this question, finding out the optimum district composition for the performance of a GS-CO2DEN system. The used cost functions, energy prices and maximal available PV area are given in Table 24.

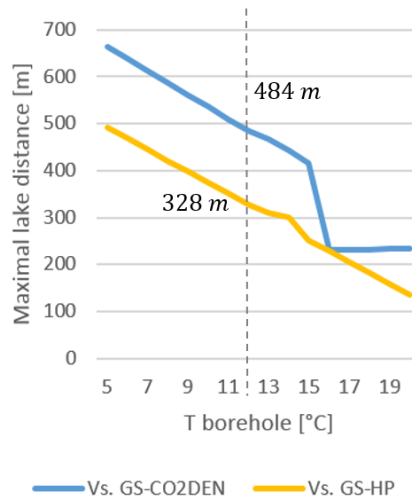


Figure 36: Maximum distance of lake for which the total costs are lower than the two other energy systems, in function of the ground temperature $T_{borehole}$. The dashed vertical line shows the values corresponding to the ground temperature in the case study

It has to be noted that, in order to focus on the energy performance of the heating and cooling energy system, the electricity consumption of the houses has been neglected in this subsection.

Table 24: Summary of relevant cost and decision constraints.

Cost functions	Table 12 in Section 4.6.1
Electricity cost	Table 13 in Section 4.6.1
Max. PV area available	2923 m^2 (see Table 8 in Section 4.4)
Electricity consumption of houses	0

As per Table 31, the building categories are:

1. Housing
2. Retail
3. Restaurant services
4. Indoor swimming pool

For sake of simplicity, among the categories shown in Table 31, the two most common and diverse - i.e. presenting the most different energy demand - have been chosen: (1) Housing -H and (2) Retail - R.

A sensitivity analysis has been performed on a district composed by those two categories. The energy demand resulting from the different combinations of the above mentioned categories is shown in Figure 37. At the far right the energy demand resulting from a district composed by 100% of retail buildings, with a decreasing share towards the left, in steps of 25%. The last column on the left is given by the Eglantine district, as a reference. It is clear to see that the retail building has a high cooling demand during summer months, with demand peaks that are around 4 times the heating demand peaks. Moreover, while the space heating demand remains very similar, the hot water demand decreases considerably.

Table 25: Comparison of energy demand and energy performance of the different combination of building use

	Eglantine	H1 / R0	H0.8 / R0.2	H0.6 / R0.4	H0.4 / R0.6	H0.6 / R0.8	H0 / R1
$Q_{heating}^+$	[MWh]	2'402	2'347	2'1614	1'976	1'790	1'603
$Q_{cooling}^+$	[MWh]	39	20	549	1'113	1'677	2'241
$Q_{GTW}^{netBalance}$	[MWh]	-1'887	-1'863	-1'195	-482	234'	951
$COP_{heating}$	[\cdot]	5.1	5.1	5.4	5.7	5.9	6.1
$COP_{cooling}$	[\cdot]	63.1	52.3	72.8	73.7	74.1	74.2
COP_{global}	[\cdot]	5.9	5.5	14.7	22.3	29.3	36.3

Table 25 shows the COP values for the energy system throughout the different combinations of buildings use. The $COP_{heating}$ increase is due to the decreasing share of DHW, which is heated with a lower COP. The increase in cooling, and thus the strong increase in the global coefficient of performance is due to the fact that the biggest share of the cooling demand can be satisfied with free-cooling. These variations are reflected in the decrease of electricity consumption, shown in the upper row of Figure 37. The resulting heat exchange with the geothermal wells is shown in the lower row of Figure 37.

Figure 38 shows the resulting costs, for the different scenarios. The operating costs decrease linearly, with the increase of the share of retail use. This is due to the smaller heating demand. The increasing cooling demand is essentially satisfied with free-cooling, which does not influence the operating cost. This means that the optimum district composition, if only the operating costs

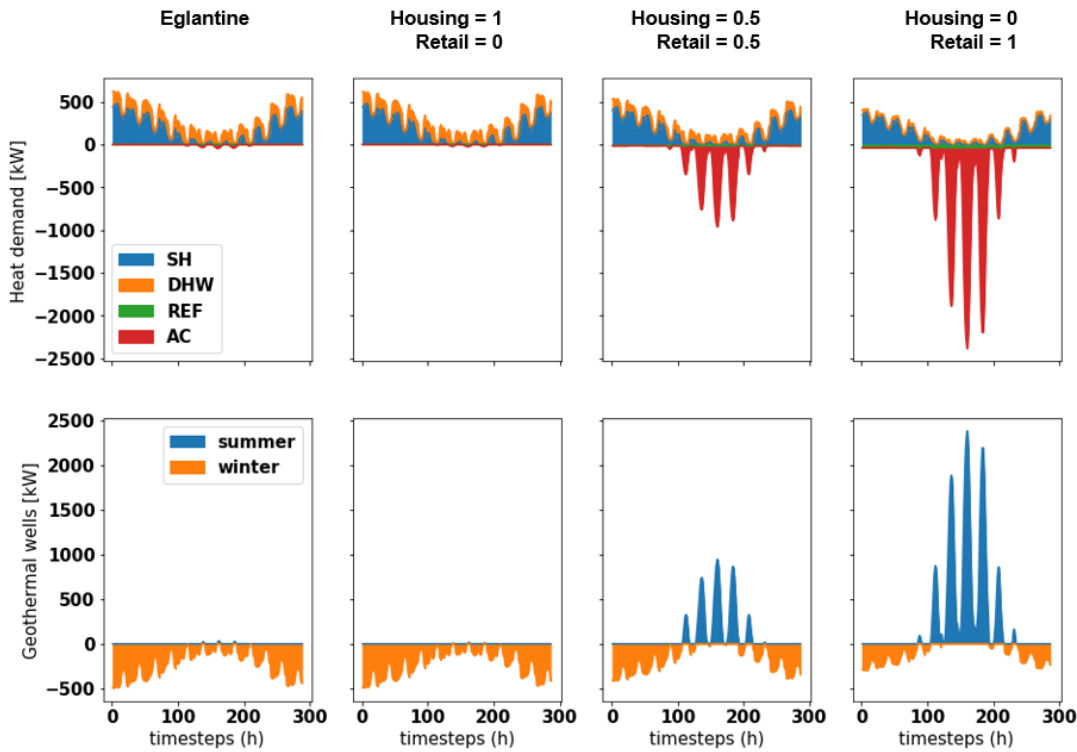


Figure 37: Comparison of the heating (+) / cooling (-) demand - upper row - and the heat extracted (+) / injected (-) into the boreholes - lower row - for different district compositions.

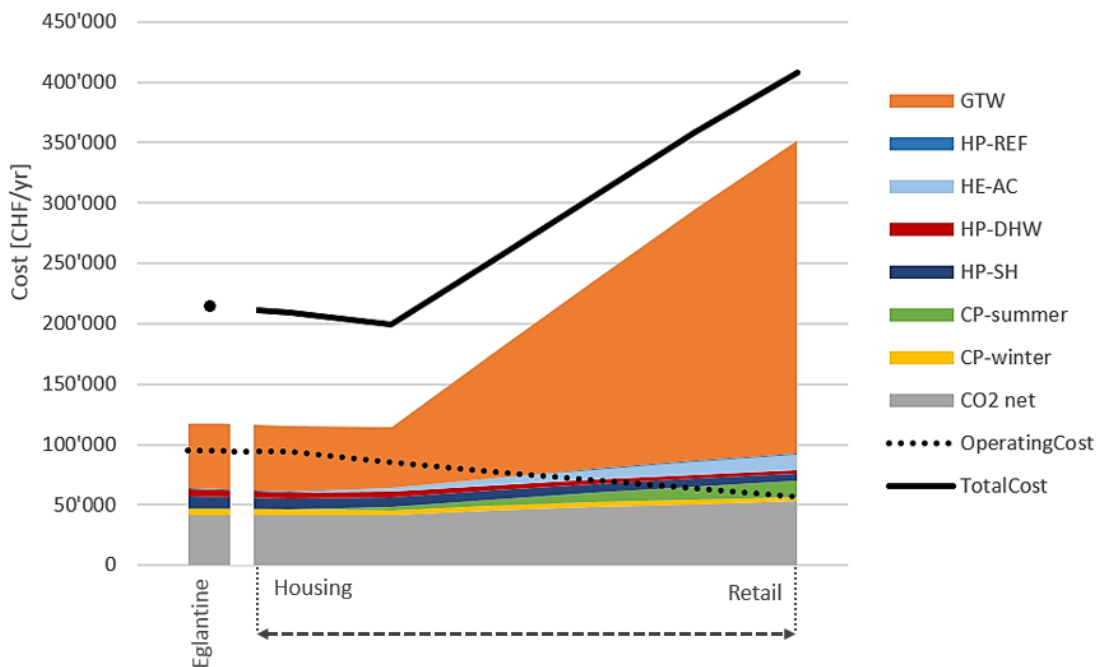


Figure 38: Cost comparison for different combinations of *housing* and *retail* building use, with the Eglantine district as a reference in the first column. The stacked columns show the investment costs.

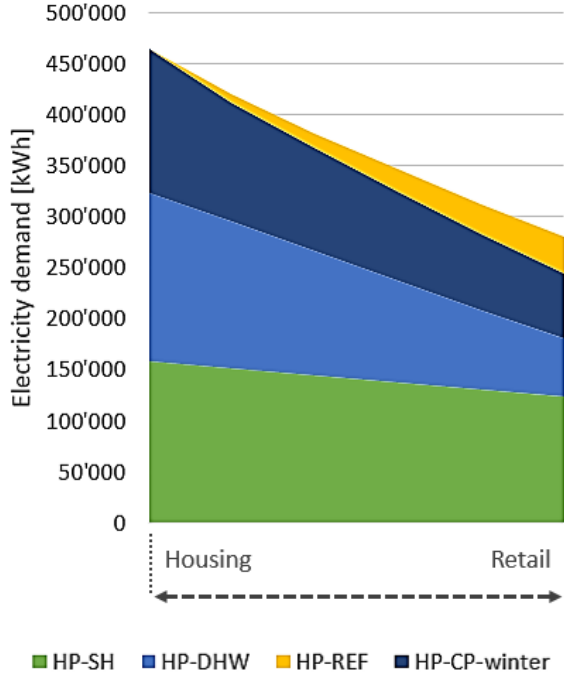


Figure 39: Electricity demand in function of the building use composition

are taken into account, is a purely retail based district.

However, the increasing amount of energy that has to be dissipated in the ground has a big impact on the investment cost, since the model sizes them in order to satisfy the peak cooling power, which is around 2000 kW for a retail composed district. In comparison, the peak heating demand in the Eglantine district sums up to 500 kW. Therefore, the increase in the IC is much bigger than the decrease of OC. In theory, the amount of heat extracted and injected in the ground should also be taken into account in the sizing of the GTW. Indeed, the geothermal field can be used as a heat storage between the seasons. In Table 25 the net heat balance over a year is shown for each combination of district use. Thus, the fact that the model in this work sizes the GTW exclusively on the peak demand, is probably resulting in an overestimation of the investment costs for the GTW.

The optimum combination of the district composition, in terms of total cost, is to be found in low shares of retail, where the cooling demand allows to partly compensate the heating demand - thus reducing the operation cost - without increasing the peak demand for the GTW. To find the precise value, a model that lets the solver choose the composition of the district has been implemented. This requires an additional set of constraints, which ensures that the chosen composition is maintained throughout all the time steps:

$$f_{h,t} = f_{h,t+1} \quad \forall t \in T, h \in H \quad (69)$$

where $f_{h,t}$ is the sizing variable of unit h in time step t (see Section 3.7) and H is a subset of units U , corresponding to the above mentioned building categories.

Every unit h in H has been sized to the total ERA of the Eglantine district. Thus, in order to have comparable results, the next constraint ensures that the share of all h sum up to the size of the Eglantine district:

$$\sum_h^H f_{h,t} = 1 \quad \forall t \in T, h \in H \quad (70)$$

The combination presenting the lowest total cost is found to be at:

$$f_{Retail} = 0.13$$

$$f_{Housing} = 0.87$$

These values are highly interesting, since they represent the typical building use in a city. This can be seen in Table 26, which shows the building use in the Zurich canton, representative example of an urban region in Switzerland. It has to be noted that the given percentages are calculated in number of buildings [53] and not function of building surface as the results in this work. The order of magnitude are nevertheless enough to prove the interest of the results.

Table 26: Building use in Zurich canton (2013) given in percentage of building number. Source: [53]

Category	Share
Housing	65%
Public	4%
Industry	4%
Logistics, retail and hospitality sector	1%
Agriculture and forestry	8%
Other	18%

To summarize, the optimum building use in districts, in function of the different objective functions, are shown in Table 27.

Table 27: Optimum district composition, in function of different optimization functions

Building Use	Eglantine	min(TC)	min(OC)
Housing	97.1%	85%	0%
Retail	1.6%	15%	100%
Restaurant services	0.8%	-	-
Indoor swimming pool	0.5%	-	-

After having analyzed the response of the system in function of the ground temperature and of different energy demands, it would be very interesting to know how the two parameters might be correlated between each other. In other words, it would be interesting to study the variation of the optimum combination of building use, in function of the borehole temperature. To do so, a sensitivity analysis has been performed on those two parameters, for the GS-HP and for the GS-CO2DEN.

To evaluate the system's performance, it has been chosen to analyze the operating costs. Given that they are directly proportional with the global COP of the energy system, they give a very good indicator of the operating conditions. The results are shown in Figures 40 and 41. It has to be noted that the z axis is scaled differently.

Figure 40 shows the performance of the GS-HP. The temperature response to a *housing* composition is decreasing with the temperature increase. This is due to the increase of COP in the decentralized HP, given the lower temperature rise to harvest heat from the ground. Moving towards a district composition with a high share of *retail* use, i.e. presenting a high space cooling and a low heating demand, the operating costs diminish, due to the lower heating demand. However, a strong increase appears for temperatures above 14 °C. The reason for this, is that the free cooling temperature threshold has been reached, requiring the use of the air cooled refrigeration system instead. This obviously engenders a considerable increase in electricity consumption, reflected in the operating cost.

The GS-CO2DEN, shown in Figure 41, shows a similar response to the temperature increase for *retail* composition, with a stronger drop once the temperature rises to the free heating threshold. This scenario had already been discussed in Section 5.4. A district dedicated entirely to retail shows a very interesting response to the ground temperature variation. The COP at very low $T_{borehole}$ increases - thus the OC decrease - with the decreasing share of heating demand and the increasing demand of free cooling. At very high $T_{borehole}$, on the contrary, the COP decreases -

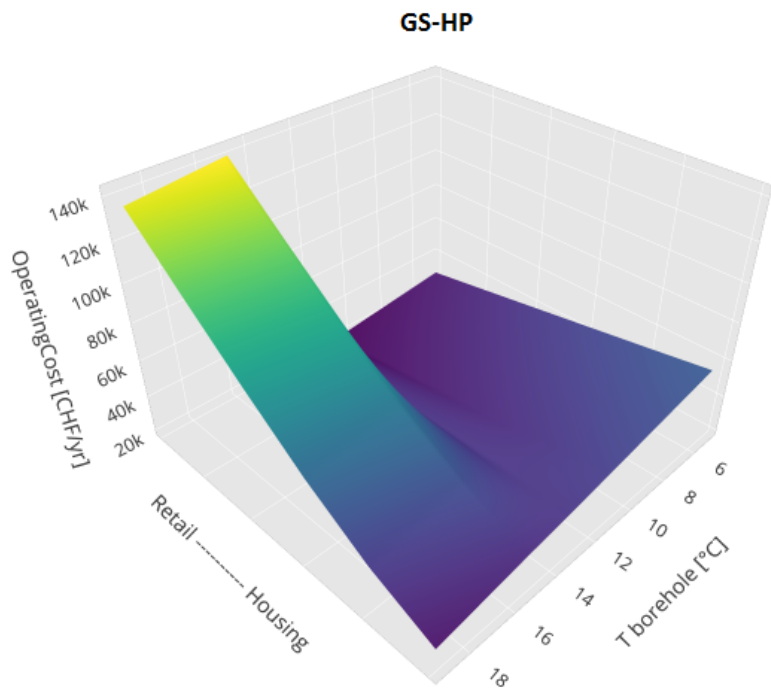


Figure 40: Operating costs in function of the borehole temperature and the building use in the district, using GS-HP technology

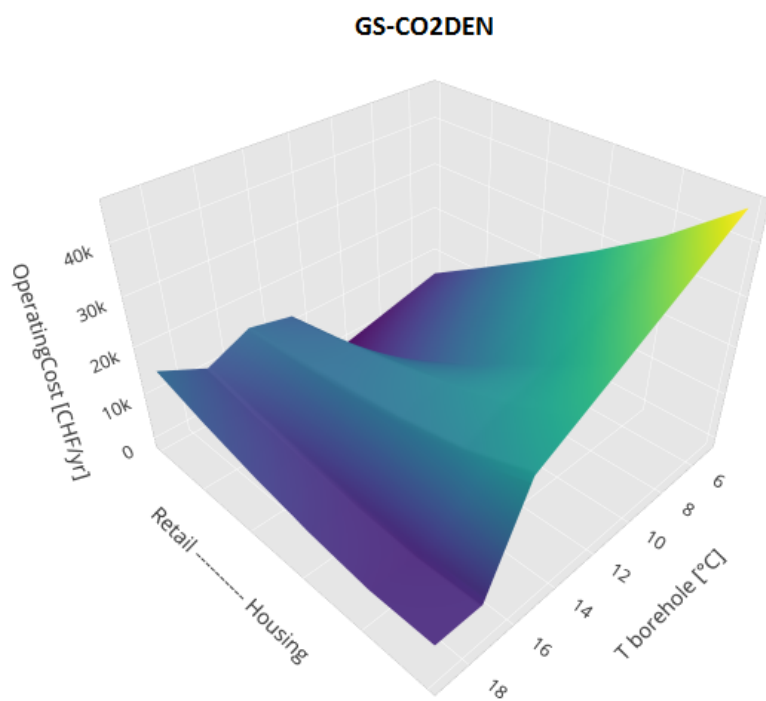


Figure 41: Operating costs in function of the borehole temperature and the building use in the district, using GS-CO2DEN technology

and OC increase - linearly with the increasing temperature drop that the refrigeration system has to perform in order to satisfy the cooling demand, which can not be free cooled. Nevertheless, the originated electricity consumption in this point is drastically lower than for the GS-HP, due to the much lower condensation temperature that has to be reached to exchange with the CO₂ network. The different operating conditions of the CP, described in Section 4.5.2, are easy to identify, thanks to the increased operating costs in between the free-cooling and free-heating threshold temperatures.

In general, the GS-CO₂DEN achieves the highest energy performance, by being as close as possible to the free heating/cooling threshold temperatures, without crossing it. Depending on the demand, it will be more efficient to be on one side or the other of the thresholds, in order to use the more needed free energy. It has to be noted that the GS-CO₂DEN performs better than the GS-HP for any given combination.

Figure 42 and 43 show the investment costs respectively for the GS-HP and the GS-CO₂DEN. Both systems present a very similar response to the two studied parameters for ground temperatures below 14°C: the investment cost increases with increasing retail share in the district, due to the higher cooling demand - which, as it has been seen, presents higher peak demand than heating demand -, and thus larger sizing of the geothermal wells. The investment costs of the GS-CO₂DEN are slightly higher due to the higher COP of the energy system, for which a larger share of the furnished energy is sourced from the ground, thus increasing the sizing of the geothermal wells.

However, the two system differ strongly for temperatures above 14°C: while the investment costs of the GS-CO₂DEN stay about constant, those of the GS-HP drop by about 30%. In the GS-HP, free cooling is replaced by air-cooled refrigeration system when the free cooling threshold is reached. This reduces drastically the sizing of the geothermal wells, and thus the total investment costs of the system.

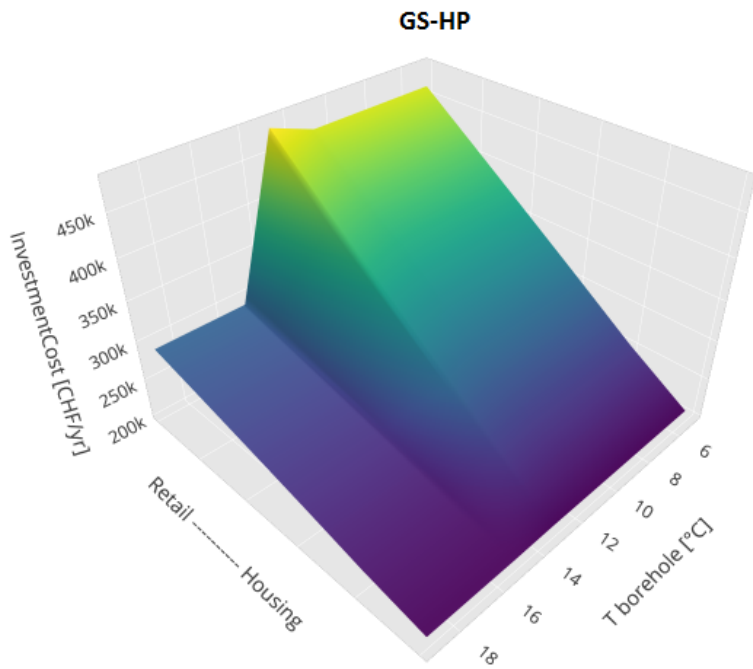


Figure 42: Investment costs in function of the borehole temperature and the building use in the district, using GS-HP technology

Figure 44 shows the difference in the resulting total cost between the two systems. Positive values mean that the GS-CO₂DEN presents a higher cost, with respect to the GS-HP. It is clear to see that the total costs strongly depend on the investment cost. Operating costs have a much smaller

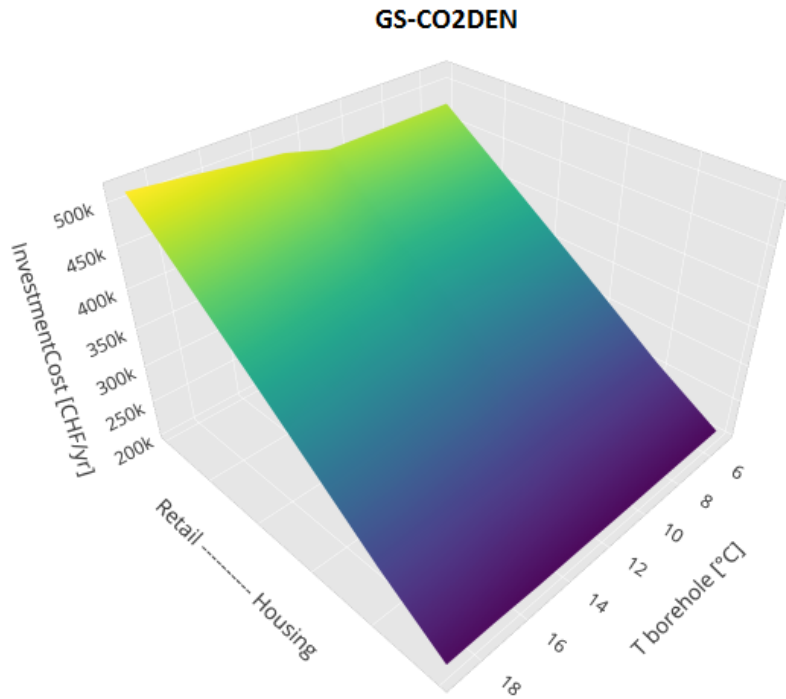


Figure 43: Investment costs in function of the borehole temperature and the building use in the district, using GS-CO2DEN technology

influence, given that its values are about one order of magnitude smaller than the investment costs.

GS-CO2DEN results to be more expensive for all combinations of district compositions and ground temperatures. However, the difference is not very relevant for temperatures below 14°C, since the difference is of about 20'000[CHF/yr]. For temperatures above 14°C the difference is strongly influenced by the drop in the investment costs of the GS-HP described in Figure 42. The larger the share of retail composition - i.e. the larger the peak cooling demand - the larger the difference in total cost - i.e. the more interesting it gets to choose the GS-HP technology.

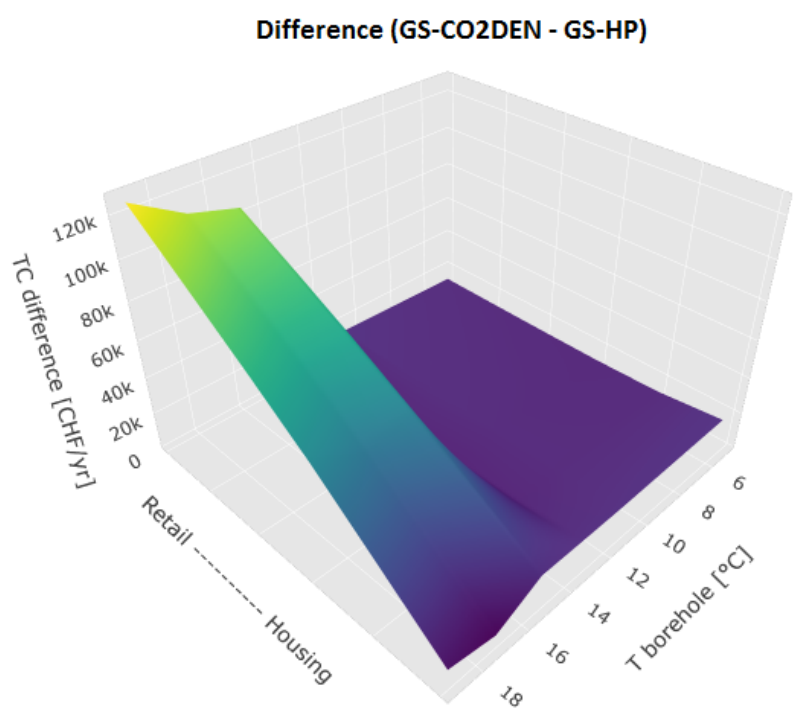


Figure 44: Difference in total cost: GS-CO2DEN - GS-HP. Negative values reflect a lower cost of the GS-CO2DEN

6 Conclusions and outlook

District energy systems have a high potential to improve the energy and exergy efficiency of urban heating and cooling systems. A particularly promising technology uses CO₂ as a working fluid to exchange heat between buildings and a network of conversion technologies. A thermo-economic analysis of the technology has been performed, focusing on a test case district near Lausanne, the Eglantine district, which is composed of 13 buildings with a total ERA of 43'350 m², and will host around 1'500 people. The building use is per 97% dedicated to housing, presenting a total heating demand of 2'350 [MWh/yr].

Three main energy conversion technologies have been considered, for the supply of heating and cooling. The first one consist in the state-of-the-art, modern energy system, based on decentralized geothermal heat pumps (GS-HP), in combination with geo-cooling and air-cooled refrigerators. This is a common choice among new built districts and houses. The other two, are CO₂ based district energy networks, connected to a set of decentralized heat pumps, and a centralized heat pump to balance out the heat of the network with the environment. One of them has the central pump exchanging heat with a geothermal field (GS-CO₂DEN), while the other exchanges heat with the lake water (SL-CO₂DEN). The different technologies have been modeled accurately, in order to have the most realistic and impartial evaluation and comparison. Moreover, the heat pump model has been improved with dynamical calculation of the compressor efficiencies.

Results showed that the best performing technology is the GS-CO₂DEN, with a global COP of 6.1 and an exergy efficiency of 22%, which is a considerable improvement with respect to the GS-HP that has a global COP of 4.6 and an exergy efficiency of 17%. This improvement is mainly due to the technology chosen for the central plant. In fact traditional geothermal heat pumps exchange heat with the ground through a secondary water loop, which is the case in the GS-HP. The CO₂ network offers the possibility to expand the refrigerant directly into the ground. This cuts the need of an additional heat exchanger and, through the use of latent heat, avoids the additional temperature rise needed in the water loop. At last, but probably most relevant, liquid CO₂ presents a greater heat transfer coefficient than water, reducing the needed minimum approach temperature to exchange with the ground from 14°C to 6.8 °C. Despite the lower compressor efficiencies for CO₂, these measures considerably reduce exergy losses and improve the COP. The LS-CO₂DEN has a slightly lower performance then the GS-CO₂DEN - global COP of 5.6 and exergy efficiency of 21% -, due to the lower temperature of the heat source.

Despite having the lowest COP, and thus the highest operating cost, the GS-HP presents the lowest total cost, with 470'000 [Euro/yr]. The reason is straightforward: the reduction in operating cost do not compensate the upfront cost of the CO₂ network, which has a total cost of 485'000 [Euro/yr]. Given the high distance to the lake (1'500 [m]), the LS-CO₂DEN presents the highest total cost, with 580'000 [Euro/yr]. A sensitivity analysis on the lake distance has shown that this technology is cheaper than the others if the district is located in direct proximity of the lake. For the Eglantine district, this is the case for water pipes shorter than 330 [m]. Thus the arguments to opt for a CO₂ network technology might not be purely financial. In fact, in cities an important argument is that often it might not be possible to drill boreholes for each building, since the space is simply not available.

One of the advantages of the CO₂ network is to recover heat from any kind of heat source. It has been shown that the integration of an ice rink, located close to the district, induces a reduction in the electricity consumption of 8%, which results in a increase in the global COP from 6.12 to 6.73. On a financial level, this reduces the needed size of the geothermal wells, but adds upfront costs for the CO₂ pipes. Summed with the reduction in operating cost, the integration of the ice rink reduces the total cost of around 4'000 [Euro/yr].

Moreover, it has been shown that for different building uses in a district, there is an optimal ground temperature, or in other words an optimal borehole depth. The GS-CO₂DEN at Eglantine conditions performs best, energetically as well as financially, at the borehole temperature of 16°C. The reasoning works also the other way around: it has been shown that, for a borehole temperature of 12 °C, the lowest total cost is given by a district composed by 85% of buildings dedicated to housing, and 15% to retail. This result is especially interesting given that the it corresponds to

the average building use of a city.

This work identifies the key parameters that the CO₂ network technology can leverage, in order to compete against modern and well performing heat pump systems. The first, and probably the most important one, is a well designed integration of the geothermal field. The second is the knowledge and understanding of the system's performance response to the different type of energy demand.

To extend and improve these analysis, it would be necessary to implement storage technologies. This would enable to improve the sizing of the equipment, and also the integration with the domestic PV production. Especially, it would be interesting to analyze the possibility to store vapor and liquid CO₂, which achieves the same effect as a battery or another heat storage. If investment cost and required storage volume are proved to be feasible and competitive, this form of storage could represent a key argument in favor of the CO₂DEN technology.

Another crucial aspect for the improvement of the presented model, are the geothermal wells. Ideally, a model should be developed, capable of accounting for the temperature gradient of the soil in function of depth, as well as the varying heat transfer coefficient of CO₂ during the different phases of the evaporation in the ground pipe [24, 49] (see Figure 49 in Appendix E). This model should also include the dependency on the heat capacity of the soil and its recharge rate [54, 49, 55] (see Figure 50 in Appendix E), which would allow to account for geothermal heat storage or borehole regeneration. Such a model would allow to improve the equipment sizing, as well as to better model the borehole's operating temperature and its dependency on the depth of the well.

Last but not least, the precision of the model should be improved by taking into account the energy needed by the circulating pumps - in the CO₂ network, the lake pipes and in the free cooling - as well as the pressure drops in the CO₂ pipes.

References

- [1] IPCC. Summary for Policymakers of IPCC Special Report on Global Warming of 1.5C approved by governments, November 2018.
- [2] Rainer Bacher. *EnergieRespekt: Der Schlüssel Für Eine Nachhaltige Energieversorgung*. Schriftenreihe Nachhaltigkeit. Faktor Verlag, Zürich, 1. auflage edition, 2014.
- [3] Dr Fatih Birol. The Future of Cooling. *IEA Publications*, page 92, 2018.
- [4] HSLU. ClimaBau - Planen angesichts des Klimawandels. Technical report, BFE, Luzern, December 2017.
- [5] United Nations Population Division and The World Bank. World Urbanization Prospects: 2018 Revision. <https://data.worldbank.org/indicator/SP.URB.TOTL.IN.ZS>.
- [6] Céline Weber and Daniel Favrat. Conventional and advanced CO₂ based district energy systems. *Energy*, 35(12):5070–5081, December 2010.
- [7] Luc Girardin. 5th generation of DHC networks - CO₂ networks, September 2018.
- [8] energie schweiz. Fallbeispiele „Thermische Netze“, February 2018.
- [9] Danfoss. Refrigerant options now and in the future, January 2017.
- [10] Hydrocarbons21.com. Switzerland to introduce HFC bans in several AC and refrigeration applications. www.hydrocarbons21.com.
- [11] European Commission for climate action. EU legislation to control F-gases. https://ec.europa.eu/clima/policies/f-gas/legislation_en, November 2016.
- [12] Alberto Cavallini. Properties of CO₂ as a refrigerant. page 17, November 2004.
- [13] Andrew Williams. In Migros's DNA. *Advancing HVAC&R naturally*, 2018.
- [14] Samuel Henchoz. Potential of refrigerant based district heating and cooling networks. page 249, March 2016.
- [15] Raluca Suciu, Luc Girardin, and François Maréchal. Energy integration of CO₂ networks and power to gas for emerging energy autonomous cities in Europe. *Energy*, 157:830–842, August 2018.
- [16] Projects in Europe - European Powertogas — European Powertogas. <http://europeanpowertogas.com/projects-in-europe/>.
- [17] Horst Kruse and Hans Russmann. The Status of Development and Research on CO₂ Earth Heat Pipes for Geothermal Heat Pumps. International High Performance Buildings Conference:9, 2010.
- [18] Yonghui Guo, Guoqiang Zhang, Jin Zhou, Jiasheng Wu, and Wei Shen. A techno-economic comparison of a direct expansion ground-source and a secondary loop ground-coupled heat pump system for cooling in a residential building. *Applied Thermal Engineering*, 35:29–39, March 2012.
- [19] Parham Eslami-Nejad, Mohamed Ouzzane, and Zine Aidoun. Modeling of a two-phase CO₂-filled vertical borehole for geothermal heat pump applications. *Applied Energy*, 114:611–620, February 2014.
- [20] Hossein Ghazizade-Ahsaee and Mehran Ameri. Energy and exergy investigation of a carbon dioxide direct-expansion geothermal heat pump. *Applied Thermal Engineering*, 129:165–178, January 2018.

- [21] Brian T. Austin and K. Sumathy. Parametric study on the performance of a direct-expansion geothermal heat pump using carbon dioxide. *Applied Thermal Engineering*, 31(17):3774–3782, December 2011.
- [22] Parham Eslami-Nejad, Mohamed Ouzzane, and Zine Aidoun. A quasi-transient model of a transcritical carbon dioxide direct-expansion ground source heat pump for space and water heating. *Applied Thermal Engineering*, 91:259–269, December 2015.
- [23] Parham Eslami-Nejad, Messaoud Badache, Arash Bastani, and Zine Aidoun. Detailed Theoretical Characterization of a Transcritical CO₂ Direct Expansion Ground Source Heat Pump Water Heater. *Energies*, 11(2):387, February 2018.
- [24] Messaoud Badache, Mohamed Ouzzane, Parham Eslami-Nejad, and Zine Aidoun. Experimental study of a carbon dioxide direct-expansion ground source heat pump (CO₂-DX-GSHP). *Applied Thermal Engineering*, 130:1480–1488, February 2018.
- [25] Luc Girardin, François Marechal, Matthias Dubuis, Nicole Calame-Darbey, and Daniel Favrat. EnerGis: A geographical information based system for the evaluation of integrated energy conversion systems in urban areas. *Energy*, 35(2):830–840, February 2010.
- [26] SIA. SIA 380/1:2016 - Besoins de chaleur pour le chauffage, December 2016.
- [27] Chanjuan Han and Xiong (Bill) Yu. Sensitivity analysis of a vertical geothermal heat pump system. *Applied Energy*, 170:148–160, May 2016.
- [28] SIA. SIA 384/6 - Sondes Geothermiques, January 2010.
- [29] Turton, Richard &C. Bailie , Richard & Whiting, Wallace. *Analysis, Synthesis and Design of Chemical Processes*. Prentice Hall, 2003.
- [30] Bin Hu, Yaoyu Li, Feng Cao, and Ziwen Xing. Extremum seeking control of COP optimization for air-source transcritical CO₂ heat pump water heater system. *Applied Energy*, 147:361–372, June 2015.
- [31] Chi-Chuan Wang. An overview for the heat transfer performance of HFO-1234yf. *Renewable and Sustainable Energy Reviews*, 19:444–453, March 2013.
- [32] Hoo-Kyu Oh and Chang-Hyo Son. Flow boiling heat transfer and pressure drop characteristics of CO₂ in horizontal tube of 4.57-mm inner diameter. *Applied Thermal Engineering*, 31(2):163–172, February 2011.
- [33] N. Mastrullo, A.W. Mauro, A. Rosato, and G.P. Vanoli. Comparison of R744 and R134a heat transfer coefficients during flow boiling in a horizontal circular smooth tube. *Renewable Energy and Power Quality Journal*, 1(07):577–581, April 2009.
- [34] Raluca Suciu, Paul Stadler, Araz Ashouri, and François Maréchal. Towards energy-autonomous cities using CO₂ networks and Power to Gas storage. In *Proceedings of ECOS 2016*, 2016.
- [35] NTB Buchs — Institut für Energiesysteme IES - Wärmepumpen Testzentrum WPZ. <https://www.ntb.ch/?id=1268>.
- [36] Jonathan Demierre, Antonio Rubino, and Jürg Schiffmann. Modeling and Experimental Investigation of an Oil-Free Microcompressor-Turbine Unit for an Organic Rankine Cycle Driven Heat Pump. *Journal of Engineering for Gas Turbines and Power*, 137(3):032602, October 2014.
- [37] Huashan Li, Fei Cao, Xianbiao Bu, Lingbao Wang, and Xianlong Wang. Performance characteristics of R1234yf ejector-expansion refrigeration cycle. *Applied Energy*, 121:96–103, May 2014.

- [38] Sung Goo Kim, Yoon Jo Kim, Gilbong Lee, and Min Soo Kim. The performance of a transcritical CO₂ cycle with an internal heat exchanger for hot water heating. *International Journal of Refrigeration*, 28(7):1064–1072, November 2005.
- [39] J. Sarkar, Souvik Bhattacharyya, and M. Ram Gopal. Simulation of a transcritical CO₂ heat pump cycle for simultaneous cooling and heating applications. *International Journal of Refrigeration*, 29(5):735–743, August 2006.
- [40] Dongfang Yang, Yulong Song, Feng Cao, Lei Jin, and Xiaolin Wang. Theoretical and experimental investigation of a combined R134a and transcritical CO₂ heat pump for space heating. *International Journal of Refrigeration*, 72:156–170, December 2016.
- [41] J Stene. Integrated CO₂ heat pump system for space heating and hot water heating in low-energy houses and passive houses. page 14, 2007.
- [42] Shouguo Wang, Hanfei Tuo, Feng Cao, and Ziwen Xing. Experimental investigation on air-source transcritical CO₂ heat pump water heater system at a fixed water inlet temperature. *International Journal of Refrigeration*, 36(3):701–716, May 2013.
- [43] Samuel Henchoz, Céline Weber, François Maréchal, and Daniel Favrat. Performance and profitability perspectives of a CO₂ based district energy network in Geneva’s City Centre. *Energy*, 85:221–235, June 2015.
- [44] Paul Stadler, Araz Ashouri, and François Maréchal. Model-based optimization of distributed and renewable energy systems in buildings. *Energy and Buildings*, 120:103–113, May 2016.
- [45] Guichet Cartographique de l’État de Vaud. <https://www.geo.vd.ch/theme/localisation.thm>.
- [46] Veille Hydro-météorologique du Canton de Vaud and TetraHydro Sarl. Morges rivière.
- [47] GADZ, CHYN, and Jules Wilhelm. Evaluation du potentiel géothermique du canton de Genève -PGG, October 2011.
- [48] Bawos.ch. Mit Erdsondenbohrungen Kosten sparen — Bauen und Wohnen in der Schweiz. <http://bawos.ch/erdsondenbohrungen-kosten-und-planung-zur-gewinnung-von-umgebungswärme/>, July 2018.
- [49] Louis Lamarche, Stanislaw Kajl, and Benoit Beauchamp. A review of methods to evaluate borehole thermal resistances in geothermal heat-pump systems. *Geothermics*, 39(2):187–200, June 2010.
- [50] Cajus Grönqvist. Comparative life-cycle cost analysis of refrigeration systems in ice rinks. page 97, August 2016.
- [51] Yann Kolasniewski. Evaluation and modelling of ice rink energy usage. page 63, 2017.
- [52] Strompreis-Webseite der ElCom: Vergleichen Sie Ihren Strompreis. <https://www.strompreis.elcom.admin.ch/>.
- [53] EnDK - Konferenz Kantonaler Energiedirektoren. Energieverbrauch von Gebäuden - Fact sheet, August 2014.
- [54] G. S. Jia, Z. Y. Tao, X. Z. Meng, C. F. Ma, J. C. Chai, and L. W. Jin. Review of effective thermal conductivity models of rock-soil for geothermal energy applications. *Geothermics*, 77:1–11, January 2019.
- [55] Heyi Zeng, Nairen Diao, and Zhaozhong Fang. Heat transfer analysis of boreholes in vertical ground heat exchangers. *International Journal of Heat and Mass Transfer*, 46(23):4467–4481, November 2003.

A Anergy nets Switzerland

Table 28: District energy systems in Switzerland [8]; n/a: not available

	Anergiennetz ETH Hönggerberg	Jardins de la Pâla	Suurstoffi- Areal	Anergiennetz Friesenberg (FGZ)	CAD La- Tour-De-Peilz	Anergiennetz- Visp	Genève-Lac- Nations (GLN)
Location	Zürich	Bulle	Rotkreuz	Zürich	La-Tour-de-Peilz	Visp	Genève
Year of construction	2012 - 2026	2012 - 2020	2010 - 2020	2011-2050	2013 - 2015	2007 - heute	2008 - 2016
Type	≤ 20 °C	≤ 20 °C	≤ 20 °C	≤ 20 °C	≤ 20°C	≤ 20 °C	≤ 20 °C
Energy Ref. Area [m²]	475'000	65'000	172'421	185'000	24 Buildings	160'000	840'000
Use	School Residential	Residential Commercial Industry	Administration Commercial Catering School	Residential Computation	Residential Administration	Residential Industry	Residential Administration School
Status	Partly built	Partly built	Partly built	Partly built	Built	Built	Built
Data Energy Consumption							
Inst. Heating capacity [kW]	8'000	2'000	6'732	3'930	10'000	3'467	4'300
Heating demand [MWh/a]	28'450	3'100	10'619	35'000	812	8'737	5'000
Inst. Cooling capacity [kW]	6'000	1'000	2'327	3'500	None	2'600	16'200
Cooling demand [MWh/a]	26'200	650	2'364	80'000	None	3'380	20'000
Heat source	Laboratories waste heat +HP	Groundwater+HP	Waste heat buildings + PVT (solar th.) +HP	Waste heat data center+HP	Lake water +HP	Inudstrial waste heat + HP	Lake water +HP
Heat storage	Geothermal well field (431 at 200m)	Groundwater 12°C	Geothermal well field (215 at 150 m, 180 at 280m)	Geothermal well field (332 at 250m)	None	None	None
Network data							
Network length [km]	1.5	0.85	2.5	1.5	4.1	4.2	6
Heating pipeT	24 °C - 8 °C	12 °C - 9 °C	25 °C - 8 °C	28 °C - 8 °C	20 °C - 6 °C	18 °C - 8 °C	17 °C - 5 °C
Cooling pipeT	4 °C - 20 °C	4 °C - 17 °C	4 °C - 17 °C	4 °C -24 °C	2 °C - 16 °C	4 °C - 16 °C	5 °C - 12 °C
Pipe diameter [mm]	DN 560	75 - 250	60 - 400	400 - 500	400 -700	DN 400	100 -700
Number of pipes	3	2	2	2	2	2	2

Table 29: District energy systems in Switzerland [8]; *n/a*: not available

	Anergienetz ETH Hönggerberg	Jardins de la Pâla	Suurstoffi- Areal	Anergienetz Friesenberg (FGZ)	CAD La- Tour-De-Peilz	Anergienetz- Visp	Genève-Lac- Nations (GLN)
Financial data							
Tot. investments [Million CHF]	37	6	n/a	42.5	32	1.26	33
Interest rate [%]	3.9 - 6.7		n/a	n/a	6.4	5.8 - 8	n/a
Lifespan [years]							
Pipes	50	30	40	50	50	40	n/a
Storage	50	None	80	50	None	None	n/a
Heating unit	20	15	20	20	25	20	n/a
Cooling unit	20	15	20	20	25	20	n/a
Cost of energy [cts.CHF/kWh]	7.7 (Heating +cooling)	5.85 – 8 (at the moment only heating)	n/a	18 (Heating)	19.8 (at the moment only heating)	22.9 (Heating + cooling)	n/a
Tot. COP of heating	7.2	4.4	n/a	5.2	n/a	n/a	n/a
Tot. COP of heating (incl. Pumps...)	5.8	2.7	2.7	4.1	3.5-4	4	6.5
Tot. EER of cooling	30.1	n/a	n/a	n/a	n/a	n/a	n/a
Tot. EER of cooling (incl. Pumps...)	6.9	12.1	n/a	n/a	n/a	n/a	n/a

B Call for tender Eglantine - details

Table 30: Estimated energy demand in call for tender

Building	Energy Ref. Area (ERA)	Inhabitants	Space Heating (SH)	Hot Water (DHW)	TOTAL
			MIINERGIE simple flux	SIA 380/1	
		[m2]	[kWh/yr]	[kWh/yr]	[kWh/yr]
1	8'200	273	245'180	170'833	416'013
2	2'615	76	82'308	50'104	132'412
3	2'415	70	76'328	45'938	122'266
4	2'780	92	83'122	57'917	141'039
5	3'700	116	113'246	74'306	187'552
6	1'500	50	44'850	31'250	76'100
7	2'870	83	90'652	54'653	145'305
8	2'500	83	74'750	52'083	126'833
9	4'225	140	126'328	88'021	214'349
10	4'455	148	133'205	92'813	226'018
11	4'190	139	125'281	87'292	212'573
12	2'300	76	68'770	47'917	116'687
13	2'300	76	68'770	47'917	116'687
14	2'300	76	68'770	47'917	116'687
TOT	46'350	1'498	1'401'559	948'958	2'350'521

Table 31: Estimated use of buildings in call for tender

Building	Housing [%]	Retail [%]	Restaurant services [%]	Indoor swimming pool [%]
1	89.58%	3.10%	4.42%	2.89%
2	97.54%	2.46%	0.00%	0.00%
3	100.00%	0.00%	0.00%	0.00%
4	100.00%	0.00%	0.00%	0.00%
5	93.19%	6.81%	0.00%	0.00%
6	95.79%	4.21%	0.00%	0.00%
7	95.79%	4.21%	0.00%	0.00%
8	100.00%	0.00%	0.00%	0.00%
9	100.00%	0.00%	0.00%	0.00%
10	100.00%	0.00%	0.00%	0.00%
11	100.00%	0.00%	0.00%	0.00%
12	100.00%	0.00%	0.00%	0.00%
13	100.00%	0.00%	0.00%	0.00%
14	100.00%	0.00%	0.00%	0.00%
Tot	97.08 %	1.63 %	0.78 %	0.51 %

Table 32: Estimated sizing of energy system in call for tender

Building	PV	HP	Geothermal	
	[kWp]	[kW]	Nb. wells	Depth [m]
1	46	223	13	284
2	45	70	4	291
3	35	64	4	269
4	33	76	5	250
5	49	100	6	276
6	55	41	3	225
7	55	77	5	256
8	37	68	4	281
9	66	115	7	271
10	0	121	7	286
11	59	114	7	269
12	33	63	4	259
13	32	63	4	259
14	27	63	4	267
TOT	570	1'258		77



Figure 45: Map of the planned Eglantine district

C CO2DEN

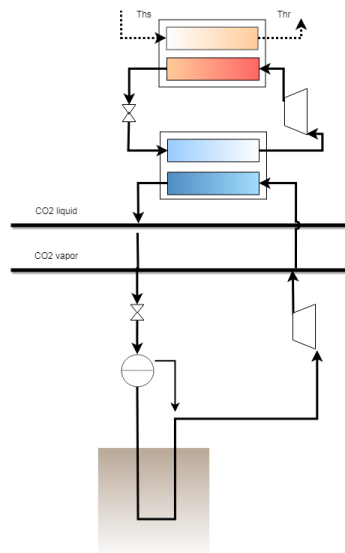


Figure 46: A simplified schematics of the CO₂ DEN with DX-GSHP technology

D Geothermal analysis for the Lemanic region

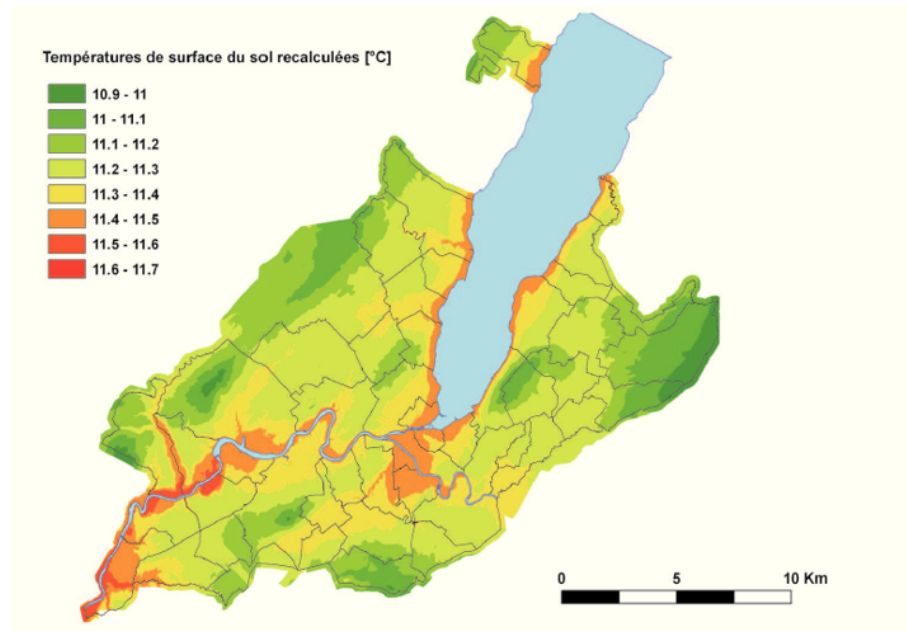


Figure 47: Surface temperature in the Lemanic region. Source: [47]

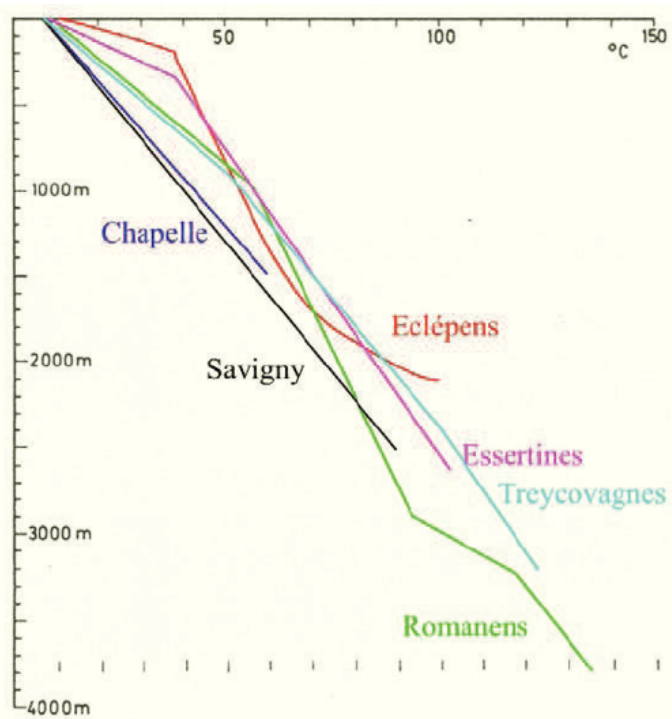


Figure 48: Temperature gradient in the ground, in function of depth, in the Lemanic region.
Source: [47]

E Geothermal models

M. Badache et al. / Applied Thermal Engineering 130 (2018) 1480–1488

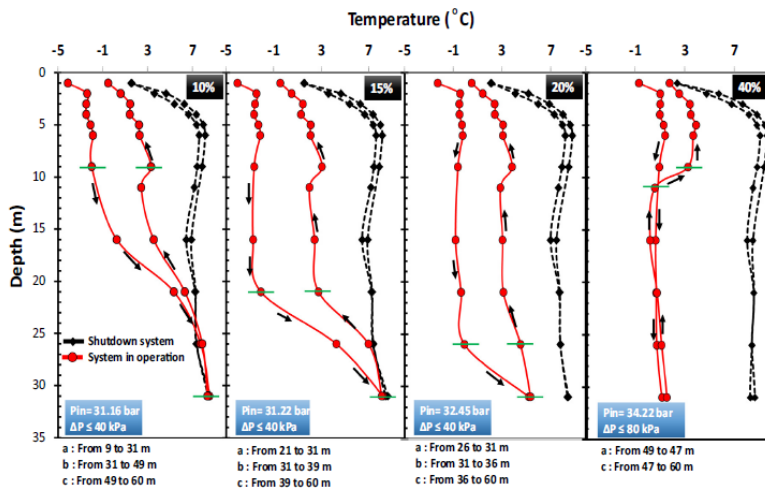


Fig. 6. Pipe wall temperature variation along the borehole as function of the opening of the EVs.

Figure 49: Pipe wall temperature variation along the borehole as function of the opening of the expansion valve, in a direct expansion GSHP. Source: [24]

M. Badache et al. / Applied Thermal Engineering 130 (2018) 1480–1488

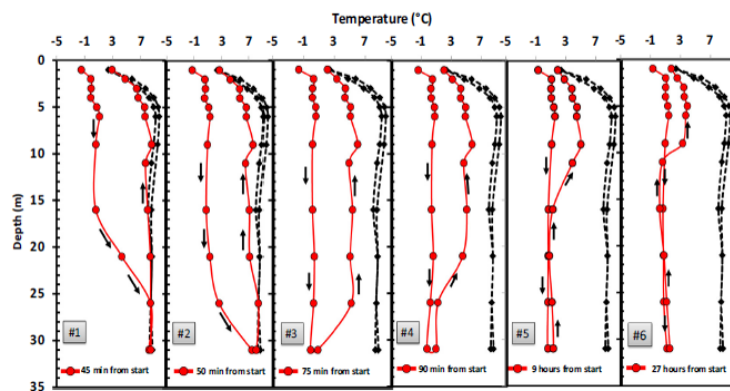


Fig. 7. Pipe wall temperature variation along the borehole at several times during heat pump operation (40% EVs opening).

Figure 50: Pipe walll temperature variation along the borehole at several times during heat pump operation, in a direct expansion GSHP. Source: [24]